Electronic Supplementary Material (ESI) for Dalton Transactions.

Supporting Information

A New Generation of Terminal Copper Nitrenes and Their Application in Aromatic C–H Amination Reactions

Fabian Thomas,[a] Matthias Oster,[a] Florian Schön,[a] Kai Göbgen,[a] Benedikt Amarouch,[a] Dominik Steden,[a] Alexander Hoffmann,[a] Sonja Herres-Pawlis*[a]

a] F. Thomas, M. Oster, Dr. F. Schön, K. Göbgen, B. Amarouch, D. Steden, Dr. A. Hoffmann, Prof. Dr. S. Herres-Pawlis
Institut für Anorganische Chemie
RWTH Aachen University
Landoltweg 1, 52074 Aachen (Germany)
E-mail:sonja.herres-pawlis@ac.rwth-aachen.de

Table of Contents

Supporting Information 0
A New Generation of Terminal Copper Nitrenes and Their Application in Aromatic C–H Amination Reactions 0
1. Experimental section 2
1.2 Cyclic voltammetry 2
1.3 Spin state measurements by the Evans' method 2
2. Characterisation of the nitrene complexes 2
2.1 Nitrene formation 2
2.2 Thermal decay 4
2.3 Ferrocene reduction 7
2.4 Cyro-UHR-ESI mass spectrometry 9
3. Catalytic reactions 12
3.1 C-H amination of toluene, ethylbenzene and cyclohexane 12
3.2 C-H amination of aromatic substrates 12
3.3 Aziridination of styrenes 13
3.4 Competitive aziridination 13
4. Crystallographic data 14
5. Key parameters determined by DFT calculation 16
6. NMR data 23

1. Experimental section

1.2 Cyclic voltammetry

Table S1: Oxidation potentials of the complexes **C1**-**C3** and **C5**.

	C1	**C2**	**C3**	**C5**
E_{ow} vs E^0 (Fc/Fc^+) [mV]	780	520	700	-290

1.3 Spin state measurements by the Evans' method

Table S2: Values of the effective magnetic moment μ_{eff} and the spin state for **N1**$^+$-**N3**$^+$. The respective calculated spin only value for μ_{eff} is 0 μ_B for a singlet, 1.73 μ_B for a doublet and 2.83 μ_B for a triplet spin state.

	N1$^+$	**N1**$^+$ (decayed)	**N2**$^+$	**N2**$^+$ (decayed)	**N3**$^+$	**N3**$^+$ (decayed)
T [°C]	-80	-10	-80	-20	-80	-30
μ_{eff} /μ_B	0.00	1.29*	0.00	0.90*	0.00	0.88*
Assigned spin state	singlet	doublet	singlet	doublet	singlet	doublet

*The decayed products are partly insoluble in DCM-d_2 and a precipitate is observed. This leads to a reduced amount of paramagnetic substance and therefore to a lower magnetic moment.

2. Characterisation of the nitrene complexes

2.1 Nitrene formation

The nitrene precursor complex ($2.63*10^{-5}$ mol,1 equiv.) was dissolved in DCM (7.0 mL) at -80 °C and titrated with ^{S}PhINTs (0.2 equiv. steps in 0.15 mL DCM up to 1.3 equiv.). After each addition of ^{S}PhINTs, the maximal UV/Vis absorption was awaited.

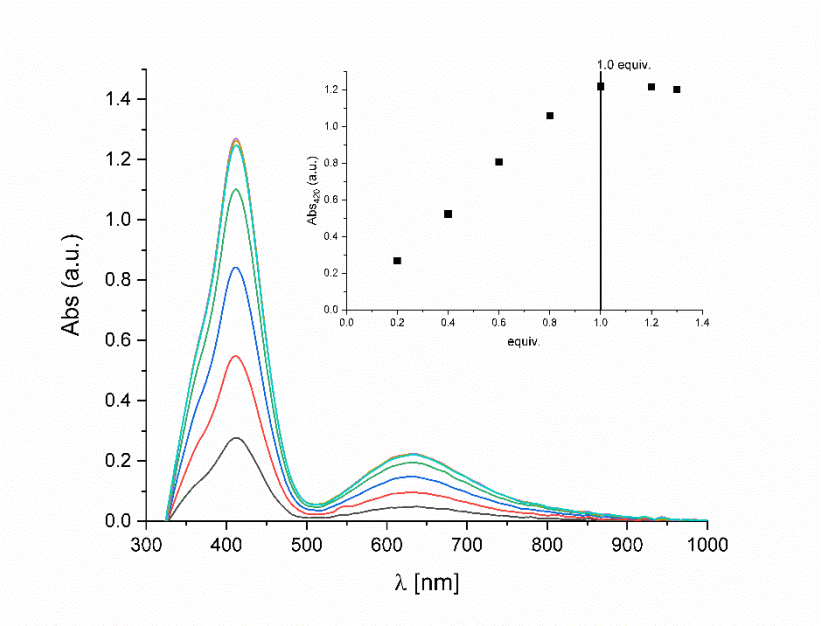

Fig. S1: Titration experiment of **C1** with ^{S}PhINTs in DCM at -80 °C.

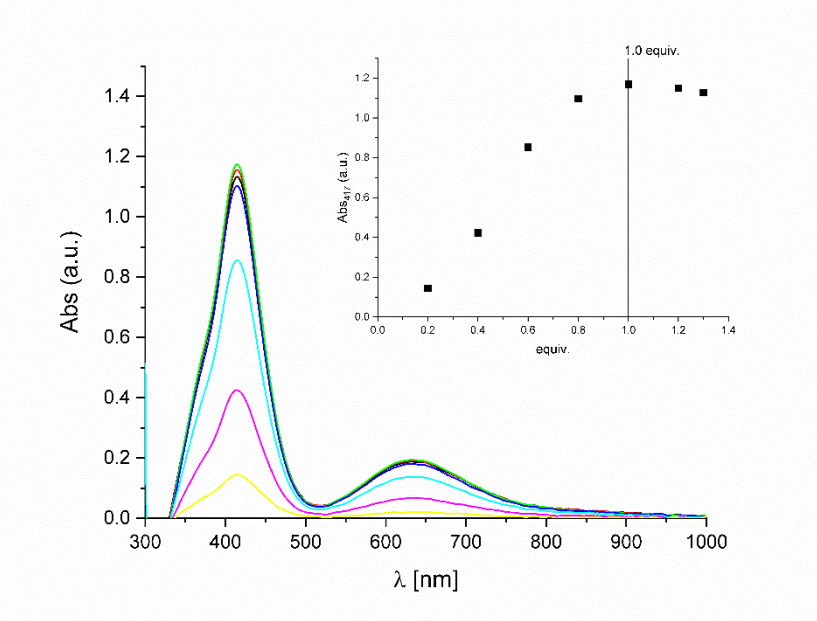

Fig. S2: Titration experiment of **C2** with ^{S}PhINTs in DCM at -80 °C.

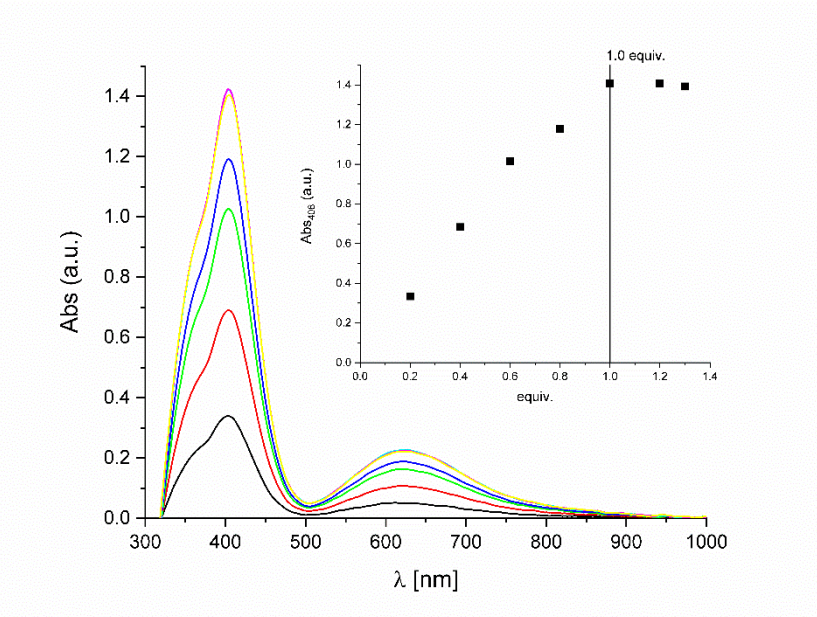

Fig. S3: Titration experiment of **C3** with ^{S}PhINTs in DCM at -80 °C.

2.2 Thermal decay

The nitrene precursor complex ($2.63*10^{-5}$ mol, 1 equiv.) was dissolved in DCM (7.0 mL) at -80 °C and ^{S}PhINTs (13.0 mg, $2.63*10^{-5}$ mol, 1 equiv.) in DCM (0.75 mL) was added. The maximal UV/Vis absorption was awaited. The thermal decay was then monitored at -42 °C.

Table S3: Half-lives for the nitrene complexes **N1**$^{+}$-**N3**$^{+}$ at -42 °C.

	N1^{+}	**N2**$^{+}$	**N2**$^{+}$ (DCM-d_2)	**N2**$^{+}$ (1.7 mM)	**N2**$^{+}$ (6.8 mM)	**N3**$^{+}$
$t_{1/2}$ [min]	50±4	5±1	6±1	2±1	25±1	42±4

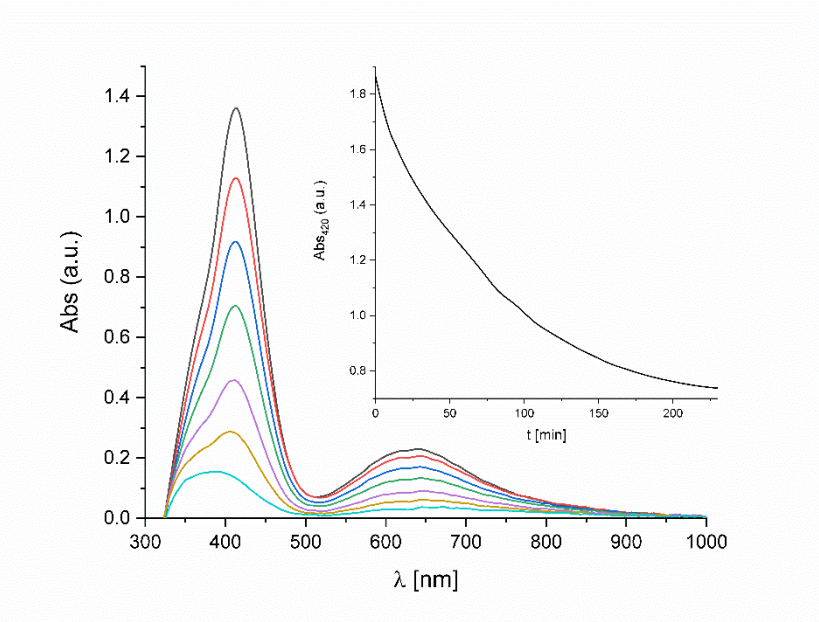

Fig. S4: Thermal decay of **N1**$^{+}$ at -42 °C in DCM. Inset: absorption trace at 420 nm.

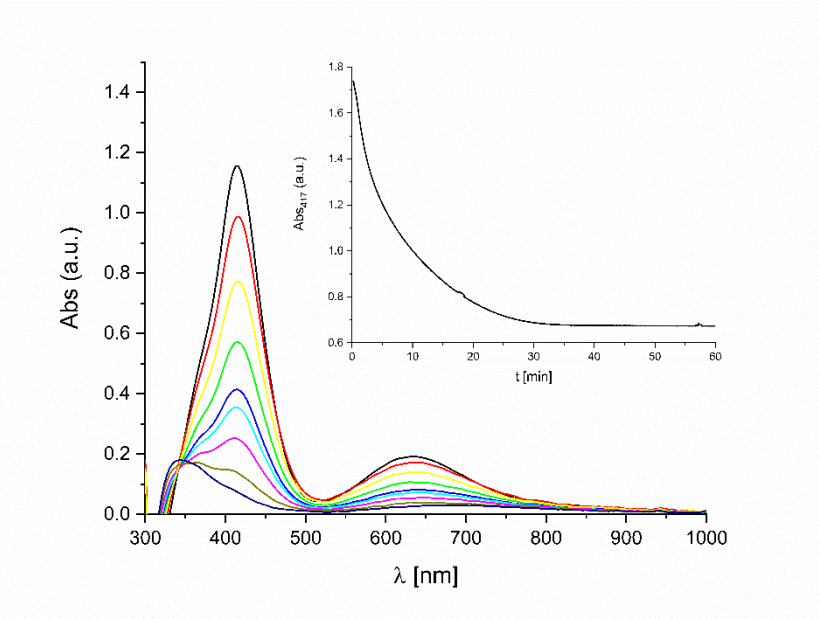

Fig. S5: Thermal decay of **N2**$^{+}$ at -42 °C in DCM. Inset: absorption trace at 417 nm.

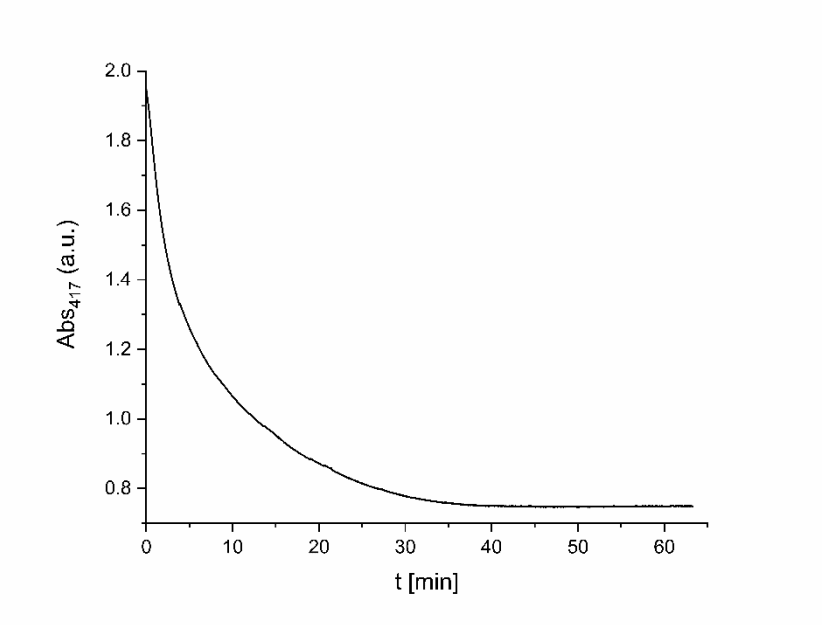

Fig. S6: Absorption trace at 417 nm of the thermal decay of **N2**$^+$ at -42 °C in DCM-d_2.

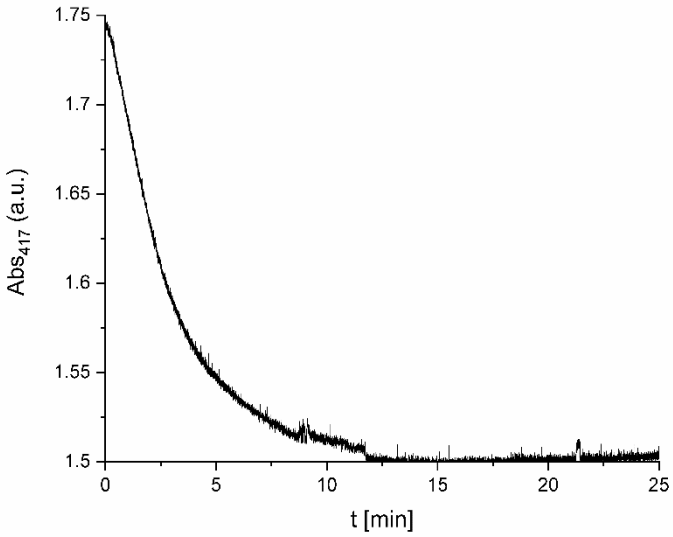

Fig. S7: Absorption trace at 417 nm of the thermal decay of **N2**$^+$ at -42 °C in DCM. Concentration: 1.7 mM.

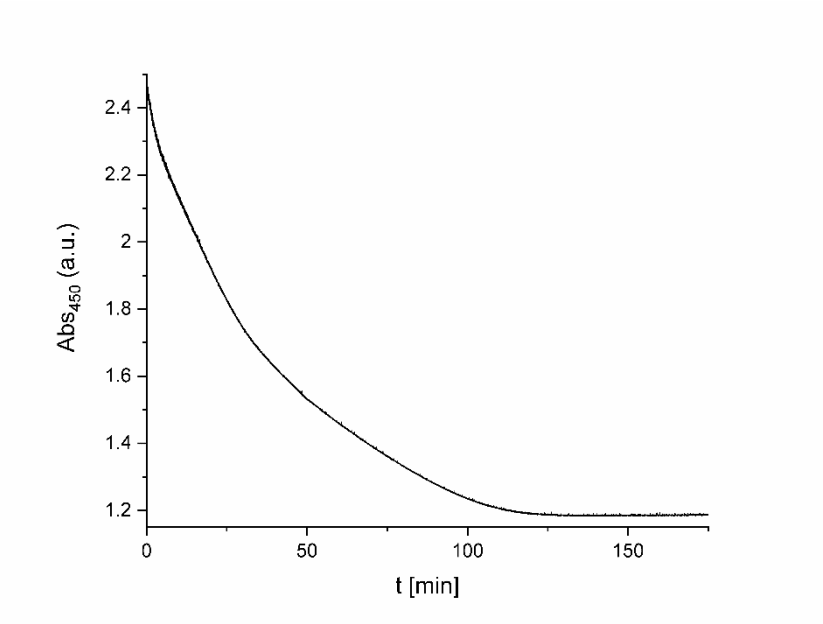

Fig. S8: Absorption trace at 417 nm of the thermal decay of **N2**$^{+}$ at -42 °C in DCM. Concentration: 6.8 mM.

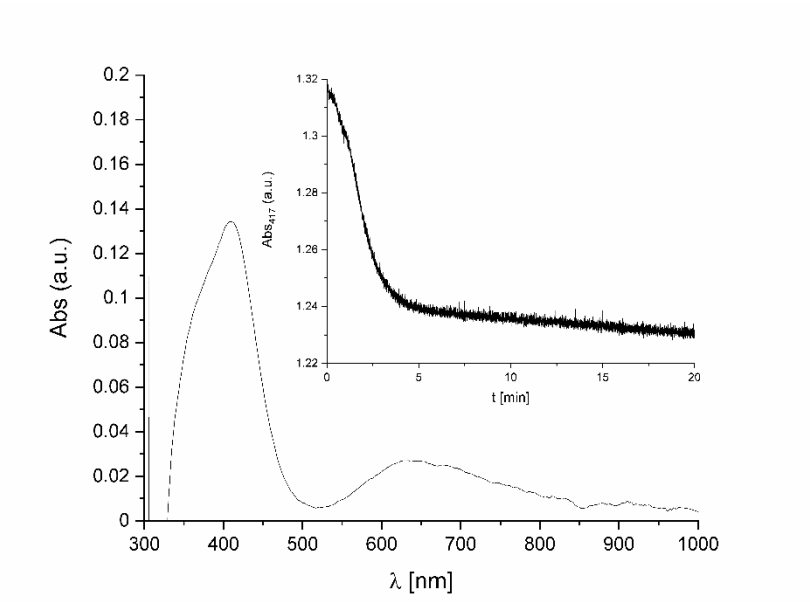

Fig. S9: Formation of **N2**$^{+}$ at -60 °C in chloroform. Inset: Absorption trace at 417 nm of the thermal decay of **N2**$^{+}$ at -42 °C

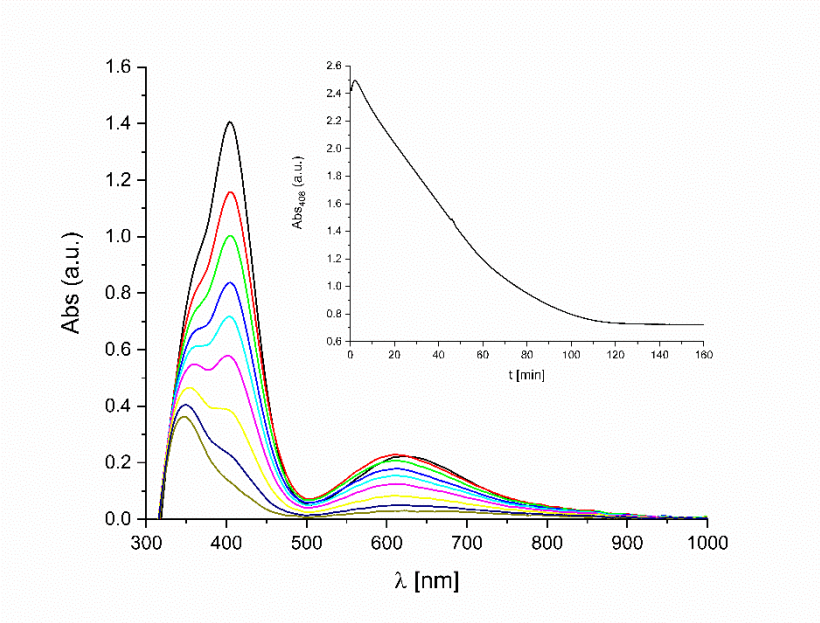

Fig. S10: Thermal decay of **N3**$^{+}$ at -42 °C in DCM. Inset: absorption trace at 408 nm.

2.3 Ferrocene reduction

The nitrene precursor complex (2.63*10^{-5} mol, 1 equiv.) was dissolved in DCM (7.0 mL) at -80 °C and ^{S}PhINTs (13.0 mg, 2.63*10^{-5} mol, 1 equiv.) in DCM (0.75 mL) was added. The maximal UV/Vis absorption was awaited. Ferrocene (146.5 mg, 7.89*10^{-4} mol, 30 equiv.) dissolved in DCM (1.0 mL) was added. The maximal UV/Vis absorption for the ferrocenium band at 624 nm was awaited. The extinction coefficient of ferrocenium (ε_{624} = 507 L*mol^{-1}*cm^{-1}) allowed the calculation of the concentration of ferrocenium from Lambert-Beer's law. This corresponds to the concentration of formed nitrene.

Table S4: Yields of the nitrene species **N1**$^{+}$-**N3** $^{+}$determined by the reduction of ferrocene.

	N1^{+}	**N2**$^{+}$	**N3**$^{+}$
$Y_{nitrene}$ [%]	89	79	90

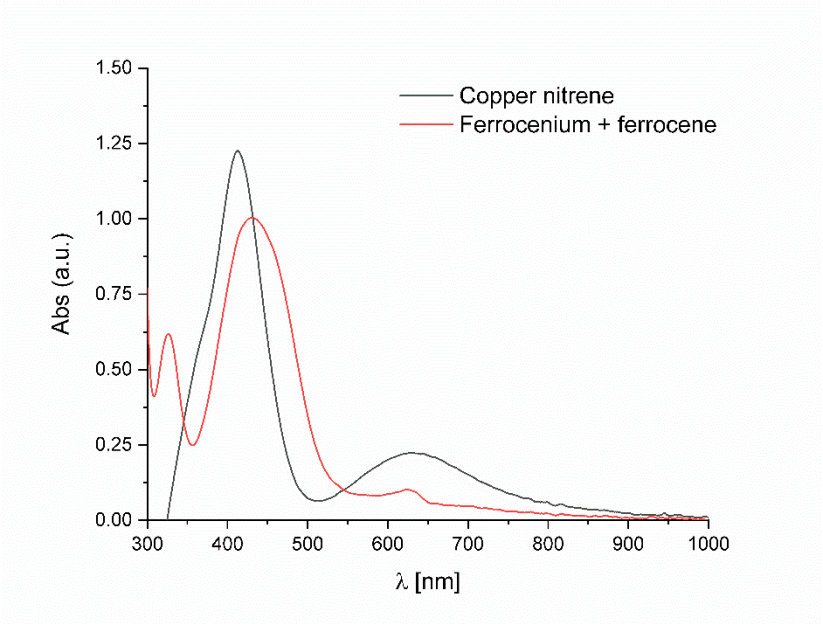

Fig. S11: Ferrocene reduction with **N1**$^{+}$.

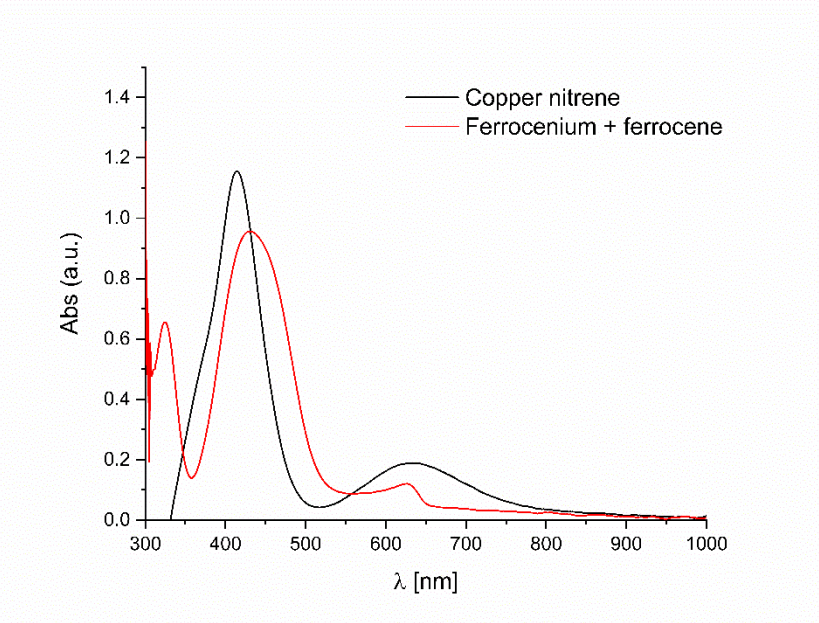

Fig. S12: Ferrocene reduction with **N2**$^{+}$.

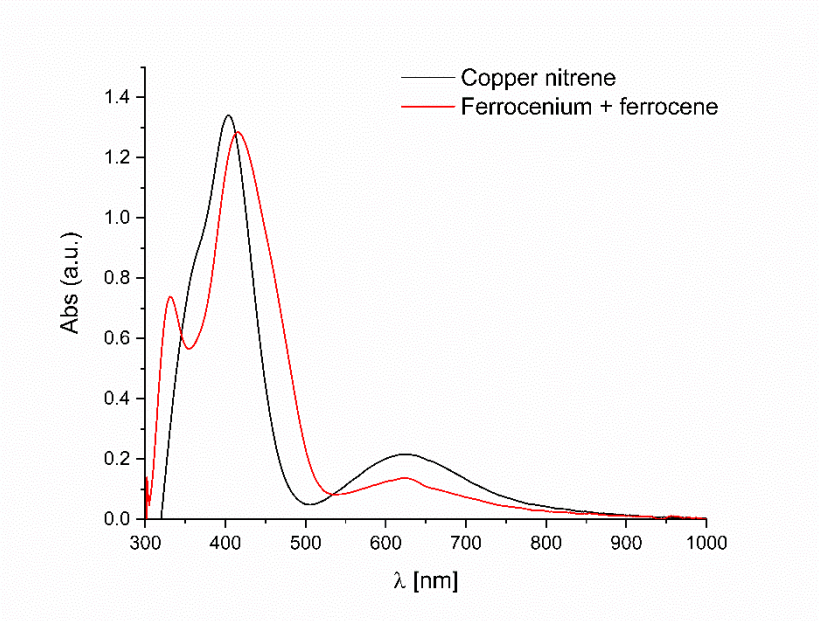

Fig. S13: Ferrocene reduction with **N3**$^{+}$.

2.4 Cyro-UHR-ESI mass spectrometry

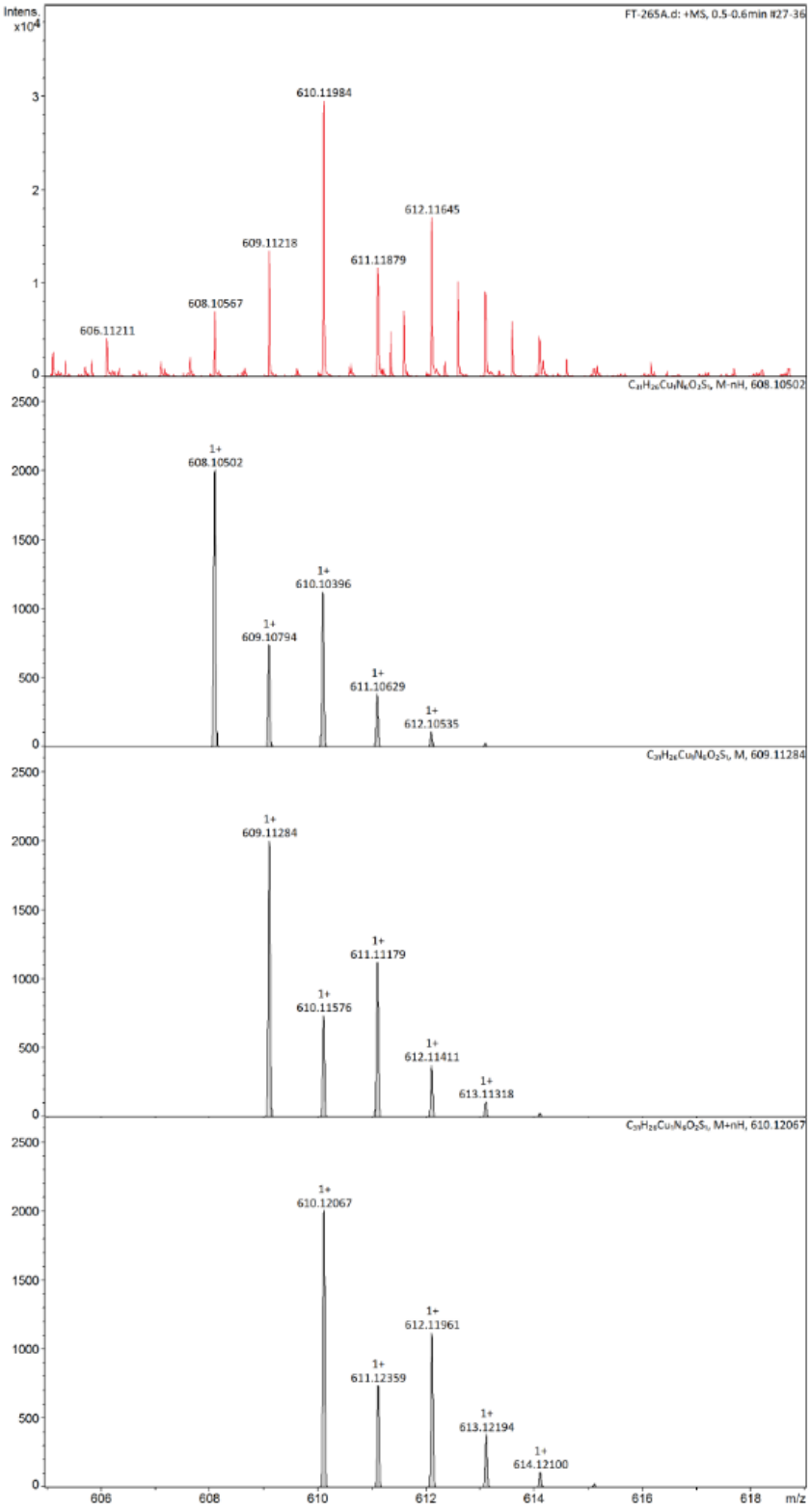

Fig. S14: Cyro-UHR-ESI mass spectrum of **N1**$^{+}$ at 183.15 K (red) and simulations of [**N1**-H]$^{+}$, **N1**$^{+}$ and [**N1**+H]$^{+}$ (black).

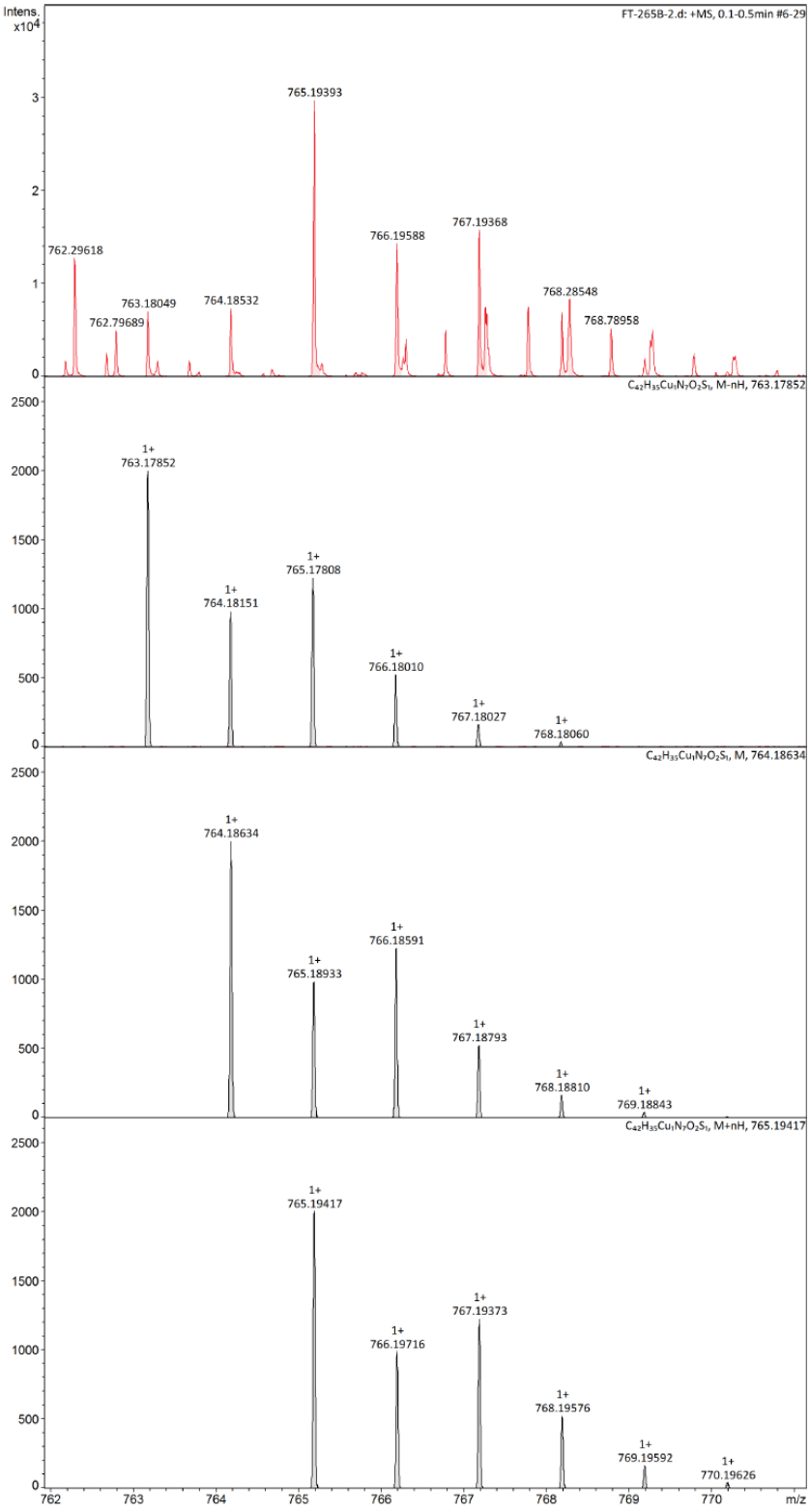

Fig. S15: Cyro-UHR-ESI mass spectrum of **N3**$^+$ at 183.15 K (red) and simulations of [**N3**-H]$^+$, **N3**$^+$ and [**N3**+H]$^+$(black).

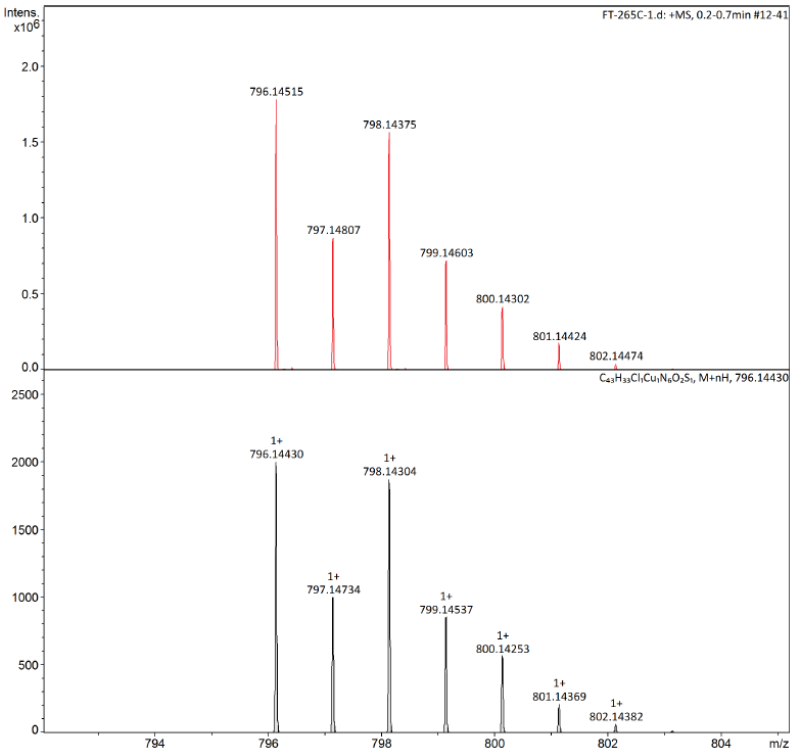

Fig. S16: Cyro-UHR-ESI mass spectrum of **N2**$^{+}$ at 183.15 K (red) and simulation of [**N2**+H]$^{+}$(black).

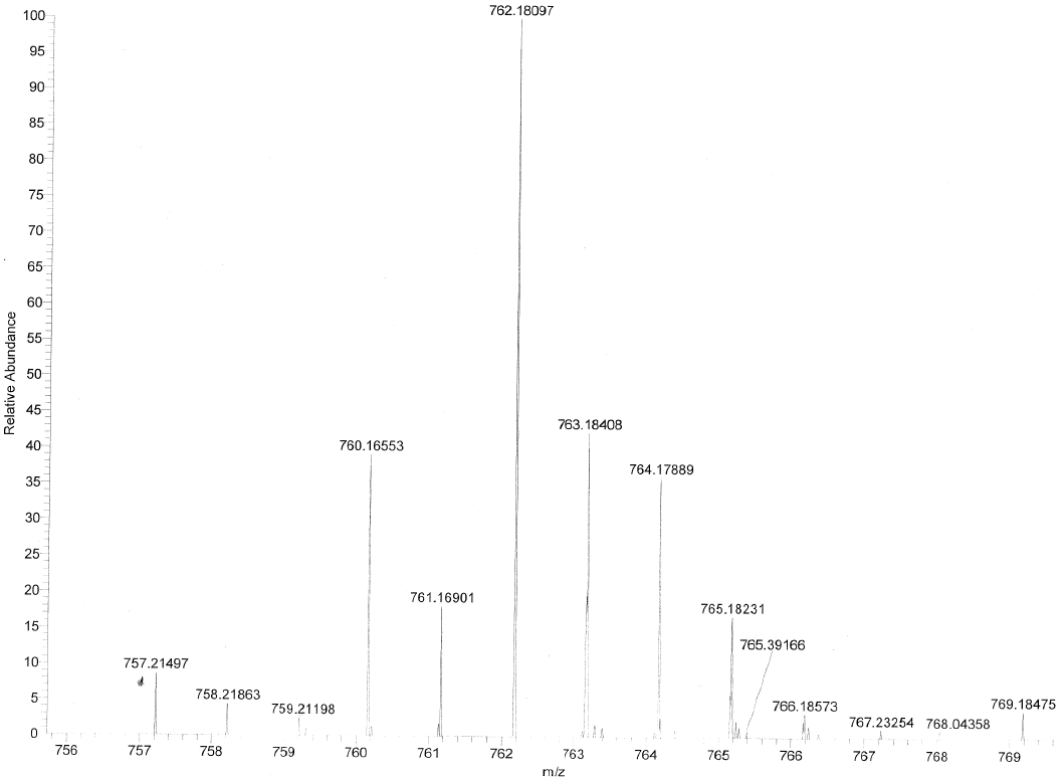

Fig. S17: ESI mass spectrum of the decay products of **N4**$^{+}$.

3. Catalytic reactions

3.1 C-H amination of toluene, ethylbenzene and cyclohexane

Table S5: Summary of the yields of the amination of benzylic and aliphatic substrates for **C1**-**C4**.

#	Catalyst	Substrate	Yield [%]
1	**C1**	Toluene	69
2	**C2**	Toluene	21
3	**C3**	Toluene	22
4	$[Cu(MeCN)_4]PF_6$	Ethylbenzene	17
5	**C1**	Ethylbenzene	49
6	**C2**	Ethylbenzene	57
7	**C3**	Ethylbenzene	10
8	**C4**	Ethylbenzene	32
9	**C1**	Cyclohexane	30
10	**C2**	Cyclohexane	18
11	**C3**	Cyclohexane	18

3.2 C-H amination of aromatic substrates

Table S6: Optimization of the reaction parameters for the amination of benzene.

#	Catalyst	Solvent ([mL])	Nitrene source	Benzene [equiv.]	Yield [%]
1	$[Cu(MeCN)_4]PF_6$	PhCl (1.0)	^{S}PhINTs	188	0
2	**C4**	PhCl (1.0)	^{S}PhINTs	188	16
3	**C4**	PhCl (0.5)	^{S}PhINTs	94	16
4	**C4**	PhCl (0.3)	^{S}PhINTs	56	17
5	**C4**	PhCl (0.5)	^{S}PhINTs	5	9
6	**C4**	-	^{S}PhINTs	188	17
7	**C4**	-	^{S}PhINTs	94	25
8	**C4**	DCM (0.5)	^{S}PhINTs	94	30
9	**C4**	DCM (0.5)	PhINTs	94	7
10	**C4**	MeCN (0.5)	^{S}PhINTs	94	35
11	**C4**	MeCN (0.5)	PhINTs	94	10
12	**C4**	MeCN (1.0)	^{S}PhINTs	188	26
13	**C4**	MeCN (0.5)	^{S}PhINTs	94	31
14	**C4**	MeCN (0.3)	^{S}PhINTs	56	37
15	**C4**	MeCN (0.5)	^{S}PhINTs	5	45
16	**C4**	MeCN (0.3)	^{S}PhINTs	5	30
17	**C1**	MeCN (0.5)	^{S}PhINTs	5	35
18	**C2**	MeCN (0.5)	^{S}PhINTs	5	24
19	**C3**	MeCN (0.5)	^{S}PhINTs	5	22

Table S7: Optimization of the reaction parameters for the amination of naphthalene.

#	Catalyst	Solvent ([mL])	Naphthalene [equiv.]	Yield [%]
1	$[Cu(MeCN)_4]PF_6$	DCM (0.5)	5	0
2	**C4**	PhCl (1.0)	5	3
3	**C4**	DCM (1.0)	5	16
4	**C4**	MeCN (1.0)	5	15
5	**C4**	DCM (0.5)	5	25
6	**C4**	MeCN (0.5)	5	27
7	**C4**	DCM (0.3)	5	18
8	**C4**	MeCN (0.3)	5	25
9	**C4**	MeCN (0.5)	10	18
10	**C1**	DCM (0.5)	5	7
11	**C2**	MeCN (0.5)	5	25
12	**C3**	MeCN (0.5)	5	23

3.3 Aziridination of styrenes

Table S8: Aziridination of styrenes with **C1**-**C4**.

#	Substrate	Equiv. (Styrene)	Equiv. (PhINTs)	Catalyst	Yield [%] (d.r. cis/trans)
1	4-NO_2-styrene	1.0	1.2	**C4**	24
2	*cis*-methylstyrene	1.0	1.2	**C4**	42 (88/12)
3	*trans*-methylstyrene	1.0	1.2	**C4**	48 (0/100)
4	styrene	1.0	1.2	**C1**	69
5	styrene[a]	1.0	1.0	**C1**	70
6	styrene[b]	2.0	1.0	**C1**	46
7	styrene[c]	3.0	1.0	**C1**	60
8	styrene[d]	4.0	1.0	**C1**	58
9	styrene[e]	5.0	1.0	**C1**	59
10	4-CF_3-styrene	1.0	1.2	**C1**	29
11	4-NO_2-styrene	1.0	1.2	**C1**	41
12	4-OMe-styrene	1.0	1.2	**C1**	14
13	*cis*-methylstyrene	1.0	1.2	**C1**	57 (86/14)
14	*trans*-methylstyrene	1.0	1.2	**C1**	45 (0/100)
15	styrene	1.0	1.2	**C2**	50
16	4-CF_3-styrene	1.0	1.2	**C2**	32
17	4-NO_2-styrene	1.0	1.2	**C2**	13
18	4-OMe-styrene	1.0	1.2	**C2**	4
19	*cis*-methylstyrene	1.0	1.2	**C2**	39 (90/10)
20	*trans*-methylstyrene	1.0	1.2	**C2**	41 (0/100)
21	styrene	1.0	1.2	**C3**	39
22	4-CF_3-styrene	1.0	1.2	**C3**	56
23	4-NO_2-styrene	1.0	1.2	**C3**	40
24	4-OMe-styrene	1.0	1.2	**C3**	7
25	*cis*-methylstyrene	1.0	1.2	**C3**	32 (63/37)
26	*trans*-methylstyrene	1.0	1.2	**C3**	47 (0/100)
27	*cis*-methylstyrene	1.0	1.2	$[Cu(MeCN)_4]PF_6$	21 (25/75)
28	*trans*-methylstyrene	1.0	1.2	$[Cu(MeCN)_4]PF_6$	30 (0/100)

[a] styrene ($1.0*10^{-4}$ mol, 1 equiv.), PhINTs ($1.0*10^{-4}$ mol, 1 equiv.); **C1** ($5*10^{-6}$ mol, 0.05 equiv.) [b] styrene ($2.0*10^{-4}$ mol, 2 equiv.), PhINTs ($1.0*10^{-4}$ mol, 1 equiv.), **C1** ($5*10^{-6}$ mol, 0.05 equiv.); [c] styrene ($3.0*10^{-4}$ mol, 3 equiv.), PhINTs ($1.0*10^{-4}$ mol, 1 equiv.), **C1** ($5*10^{-6}$ mol, 0.05 equiv.); [d] styrene ($4.0*10^{-4}$ mol, 4 equiv.), PhINTs ($1.0*10^{-4}$ mol, 1 equiv.), **C1** ($5*10^{-6}$ mol, 0.05 equiv.); [e] styrene ($5.0*10^{-4}$ mol, 5 equiv.), PhINTs ($1.0*10^{-4}$ mol, 1 equiv.), **C1** ($5*10^{-6}$ mol, 0.05 equiv.).

3.4 Competitive aziridination

Table S9: Competitive aziridination between styrene and *para*-subsituted styrene derivatives by **C1** and PhINTs in DCM at 30 °C.

R	σ_{jj} [S1]	σ_{mb} [S1]	σ^+ [S1]	av. k_X/k_H	log(av. k_X/k_H)	
H	0	0	0	1	0	0
F	-0.02	-0.24	-0.07	1.20±0.09	0.081±0.033	0.064
Cl	0.22	0.11	0.11	1.22±0.03	0.086±0.011	0.057
Br	0.23	0.13	0.15	1.18±0.06	0.072±0.023	0.055
CF_3	-0.01	0.49	0.61	0.72±0.03	-0.142±0.021	-0.152
NO_2	0.36	0.86	0.79	0.58±0.05	-0.233±0.035	-0.111
^{t}Bu	0.26	-0.22	-0.26	1.75±0.24	0.243±0.052	0.173
Me	0.15	-0.29	-0.31	1.29±0.04	0.111±0.015	0.149
OMe	0.23	-0.77	-0.78	2.04±0.25	0.310±0.052	0.326

[S1] a) V. Bagchi, P. Paraskevopoulou, P. Das, L. Chi, Q. Wang, A. Choudhury, J. S. Mathieson, L. Cronin, D. B. Pardue, T. R. Cundari, G. Mitrikas, Y. Sanakis, P. Stavropoulos, *J. Am. Chem. Soc.* **2014**, *136*, 11362. b) X. Jiang, G. Ji, *J. Org. Chem.* **1992**, *57*, 6051; c) X.-K. Jiang, W. W. Liu, S. Wu, *J. Phys. Org. Chem.* **1994**, *7*, 96.

4. Crystallographic data

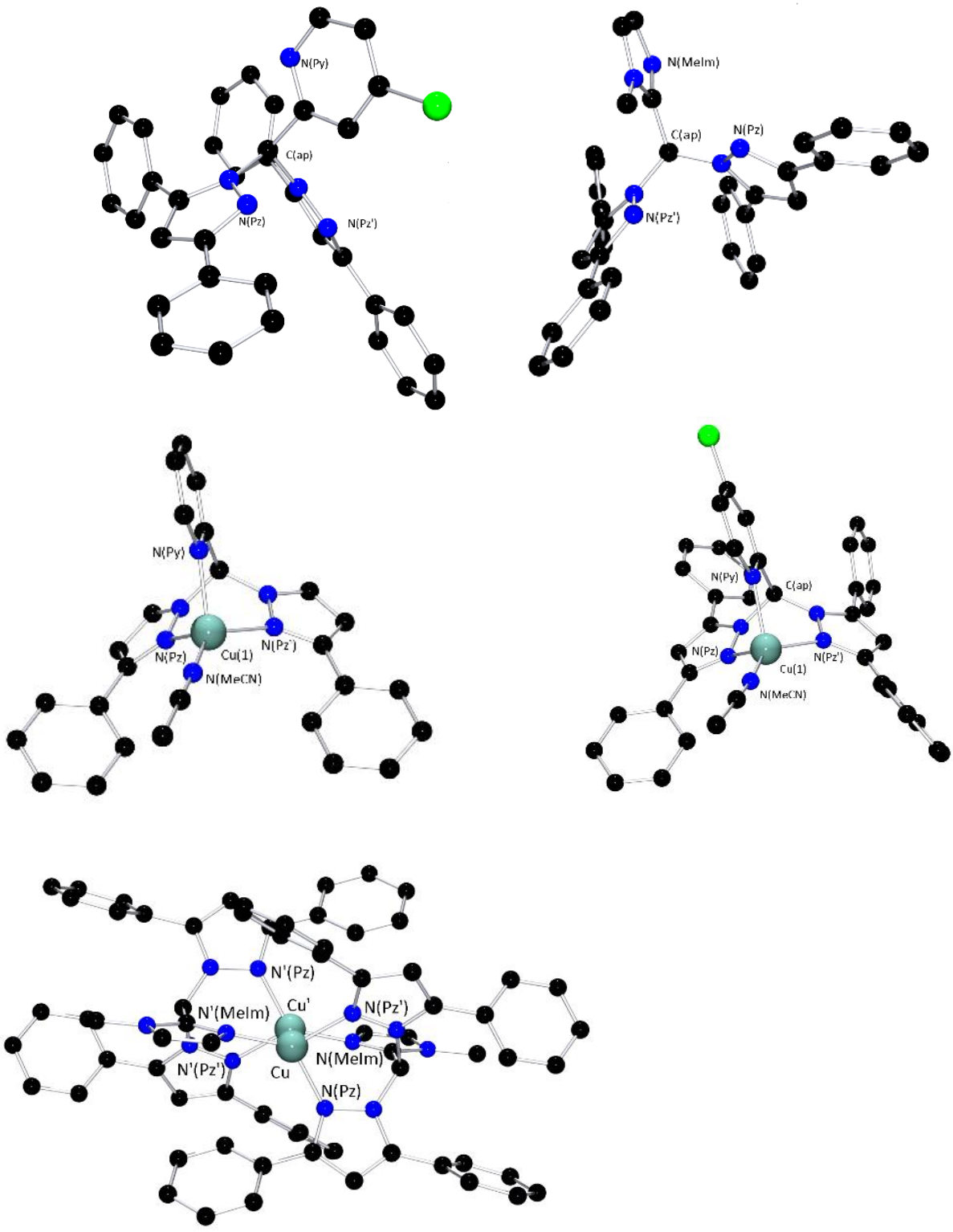

Fig. S18: Molecular structures of **L2**, **L3** and the cations of**C1**, **C2** · 1.5 DCM and **C5** · **4 CHCl₃** in the solid state. The hydrogen atoms, solvent molecules and counterions were omitted for clarity.

Table S10: Crystallographic data and parameters for **L2**, **L3**, **C1**, **C2** and **C5**.

	L2	**L3**	**C1**	**C2 · 1.5 DCM**	**C5 · 4 $CHCl_3$**
Empirical formula	$C_{36}H_{26}ClN_5$	$C_{35}H_{28}N_6$	$C_{26}H_{22}CuF_6N_6P$	$C_{79}H_{64}Cl_8Cu_2F_{12}N_{12}P_2$	$C_{74}H_{60}Cl_{12}Cu_2F_{12}N_{12}P_2$
Formula weight [g mol^{-1}]	564.07	532.63	627.00	1882.04	1959.76
Crystal size [mm]	0.33 x 0.26 x 0.17	0.32 x 0.29 x 0.28	0.44 x 0.33 x 0.22	0.21 x 0.13 x 0.08	0.14 x 0.12 x 0.10
T [K]	100	100	100	100	100
Crystal system	triclinic	monoclinic	monoclinic	triclinic	monoclinic
Space group	$P\bar{1}$	$P2_1/c$	$P2_1/n$	$P\bar{1}$	$P2_1/c$
a [Å]	11.375(2)	11.707(4)	12.778(3)	11.931(2)	11.877(2)
b [Å]	11.866(2)	21.831(7)	13.899(3)	15.931(3)	18.917(4)
c [Å]	12.420(3)	11.757(4)	16.116(3)	21.581(4)	18.418(4)
α [°]	107.92(3)	90	90	89.59(3)	90
β [°]	106.74(3)	113.371(7)	112.11(3)	76.64(3)	96.14(3)
γ [°]	101.25(3)	90	90	87.33(3)	90
V [$Å^3$]	1451.3(6)	2758.3(15)	2651.8(11)	3986.6(15)	4114.2(15)
Z	2	4	4	2	2
$P_{cacld.}$ [g cm^{-3}]	1.291	1.283	1.570	1.568	1.582
μ [mm^{-1}]	0.166	0.078	0.955	4.205	1.024
λ [Å]	0.71073	0.71073	0.71073	1.54186	0.71073
F(000)	588	1120	1272	1908	1976
hkl range	±13, ±14, ±14	±14, ±26, ±14	±15, ±16, ±19	-12 ≤ h ≤ 14, -11 ≤ k ≤ 19, -26 ≤ l ≤ 25	-16 ≤ h ≤ 17, -20 ≤ k ≤ 27, ±27
Reflections collected	16224	25280	28696	23297	50395
Independent reflections	5328	4760	4884	12881	13673
$R_{int.}$	0.0940	0.1257	0.0867	0.1012	0.0881
Number of parameters	379	371	362	1038	515
R_1 *[I≥2σ[I]]*	0.0600	0.0506	0.0448	0.0823	0.0503
wR_2 (all data)	0.1606	0.1157	0.1195	0.2393	0.1073
Goodness-of-fit	1.008	0.792	1.034	0.978	0.811
Largest diff. peak, hole [e$Å^{-3}$]	0.385, -0.368	0.221, -0.255	0.660, -0.507	0.881. -1.168	1.723, -1.130

Table S11: Selected bond lengths and angles for **L2**, **L3**, **C1**, **C2** and **C5**.

	L2	**L3**	**C1**	**C2**	**C5**
C(ap)–N(Pz, Pz') [Å]	1.458(4), 1.461(4)	1.456(3), 1.464(3)	1.458(4), 1.456(4)	1.473(9), 1.456(9)	1.452(3), 1.463(3)
C(ap)–C(Py/Im) [Å]	1.521(4)	1.509(3)	1.515(4)	1.514(10)	1.499(4)
Cu–NCMe [Å]			1.872(3)	1.888(6)	-
Cu–N(Pz, Pz') [Å]			2.066(3), 2.067(3)	2.047(6), 2.116(6)	2.014(2), 1.979(2)
Cu–N(Py/Im) [Å]			2.090(3)	2.124(6)	1.913(2)
Cu–Cu' [Å]			-	-	2.568(1)
Cu'/MeCN–Cu–N(Pz, Pz') [°]			122.2(1), 132.3(1)	142.1(3), 123.4(3)	89.4(1), 99.7(1)
Cu'/MeCN–Cu–N(Py/Im) [°]			123.3(1)	109.6(3)	99.2(1)
N(Pz, Pz')–Cu–N(Py/Im) [°]			89.0(1), 89.6(1)	90.7(2), 89.1(2)	132.0(1), 130.4(1)
τ_4			0.74	0.67	0.69

5. Key parameters determined by DFT calculation

Table S12: Key geometric parameters of the cationic species of the complexes **C1** – **C3** and **C5** (Gaussian16; TPSSh/def2-TZVP and PCM solvent model for dichloromethane and the empirical dispersion correction with Becke-Johnson damping).

	C1$^+$	**C2$^+$**	**C3$^+$**	**C5$^+$**
Bond lengths [Å]				
Cu – N(Pz. Pz')	2.070/2.070	2.057/2.068	2.092/2.128	1.978/2.024
Cu – N(Py/Im)	2.099	2.105	2.057	1.930
Cu – N($NCCH_3$)	1.871	1.870	1.866	
Cu…Cu				2.530

Table S13: NBO charges (in e^- units) and charge transfer energies (in kcal/mol) for selected atoms (*italic*) for the cationic species of a**C1** – **C3** and **C5** (NBO6.0. TPSSh/def2-TZVP and PCM solvent model for dichloromethane and the empirical dispersion correction with Becke-Johnson damping).

	C1$^+$	**C2$^+$**	**C3$^+$**	**C5$^+$**
NBO charges				
Cu	0.94	0.94	0.93	0.88
N(Pz/Pz')	-0.37 / -0.37	-0.37 / -0.37	-0.36 /-0.36	-0.41 /-0.40
N(Py/Im)	-0.52	-0.52	-0.55	-0.58
N($NCCH_3$)	-0.52	-0.53	-0.52	
Charge transfer energies				
N(Pz/Pz') → Cu	25.7 / 25.2	24.3 / 26.0	22.5 / 20.2	21.7 / 26.3
N(Py/Im) → Cu	19.8	19.5	26.3	32.2
N($NCCH_3$) → Cu	46.3	46.2	45.8	

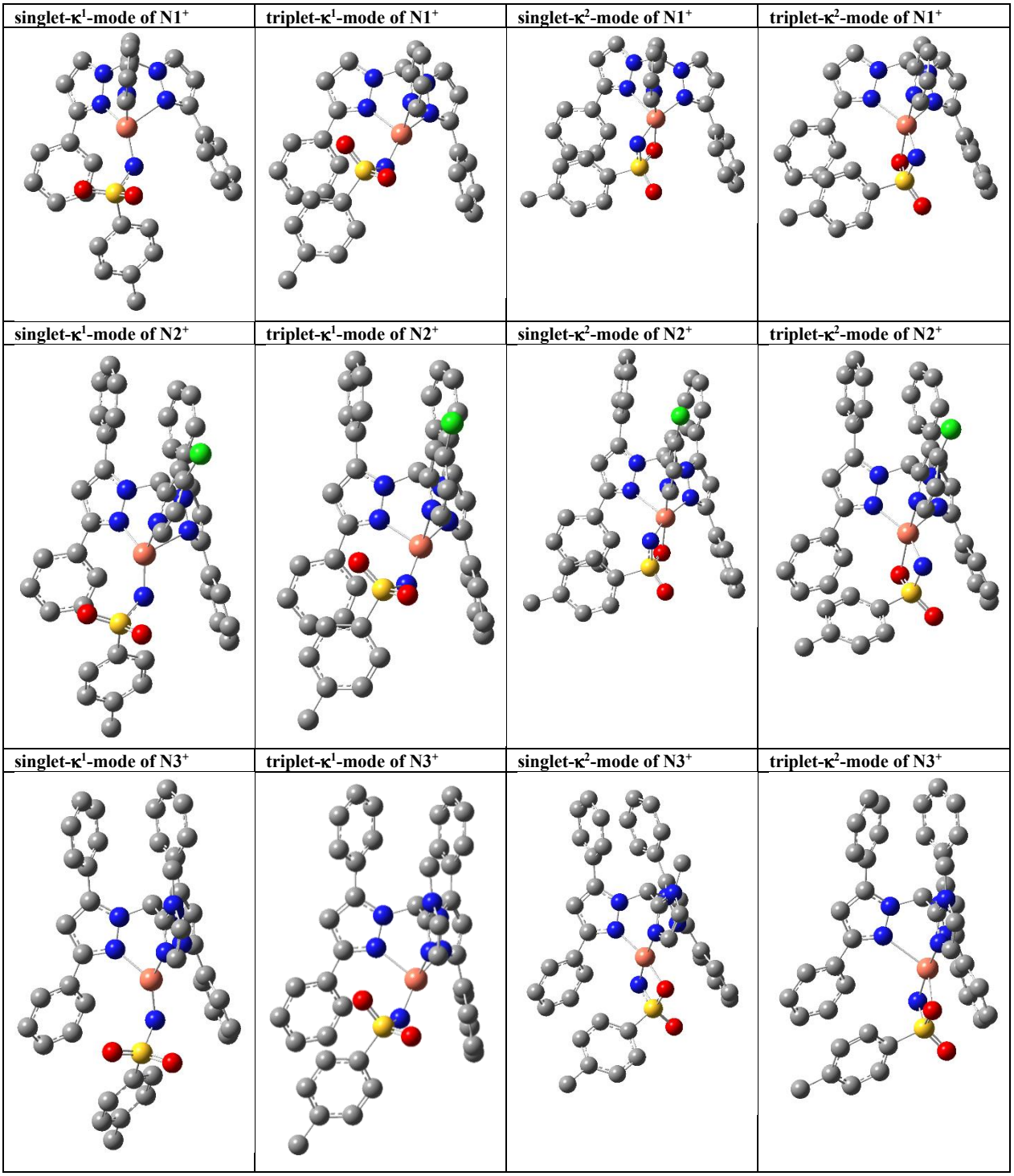

Fig. S19: κ^1- and κ^2-coordination motifs of the nitrene moieties in the copper nitrenes of the optimized structures (TPSSh/def2-TZVP and PCM solvent model for dichloromethane and the empirical dispersion correction with Becke-Johnson damping).

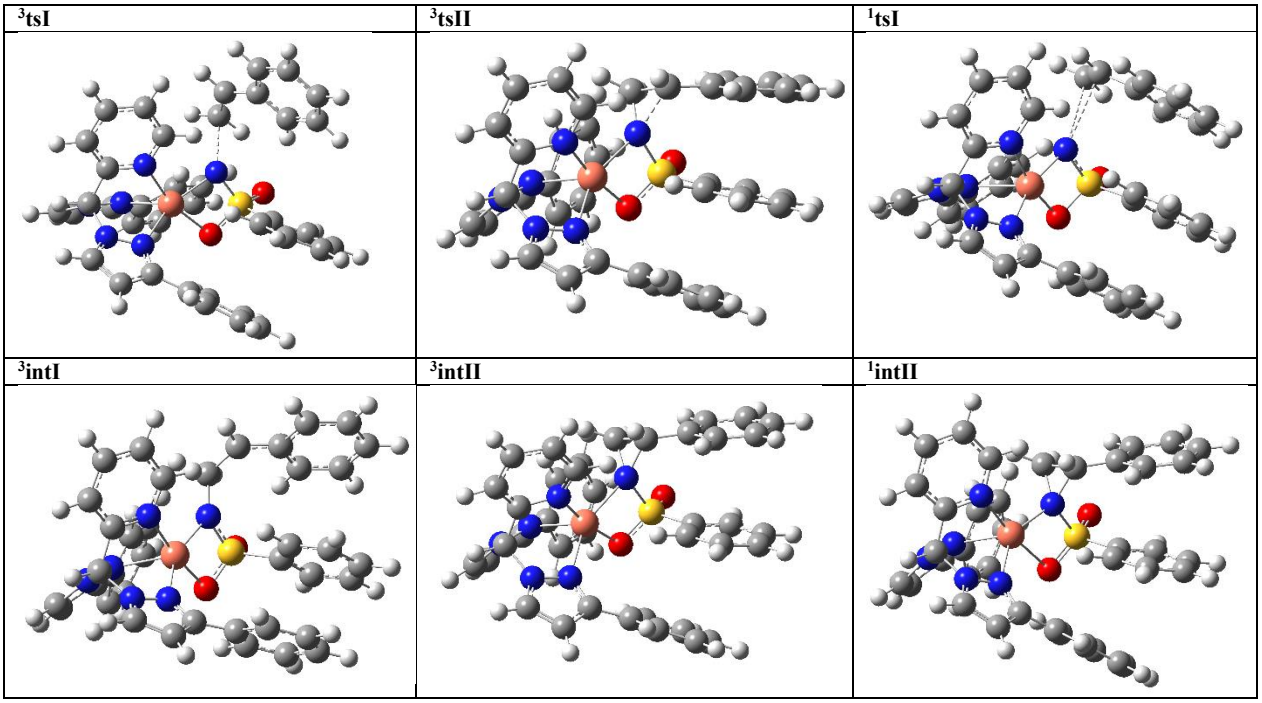

Fig. S20: Optimized structures of the proposed reaction mechanism of the aziridination reaction of styrene with **N1**$^+$ obtained at TPSSh/def2-SVP and the empirical dispersion correction with Becke-Johnson damping level of theory.

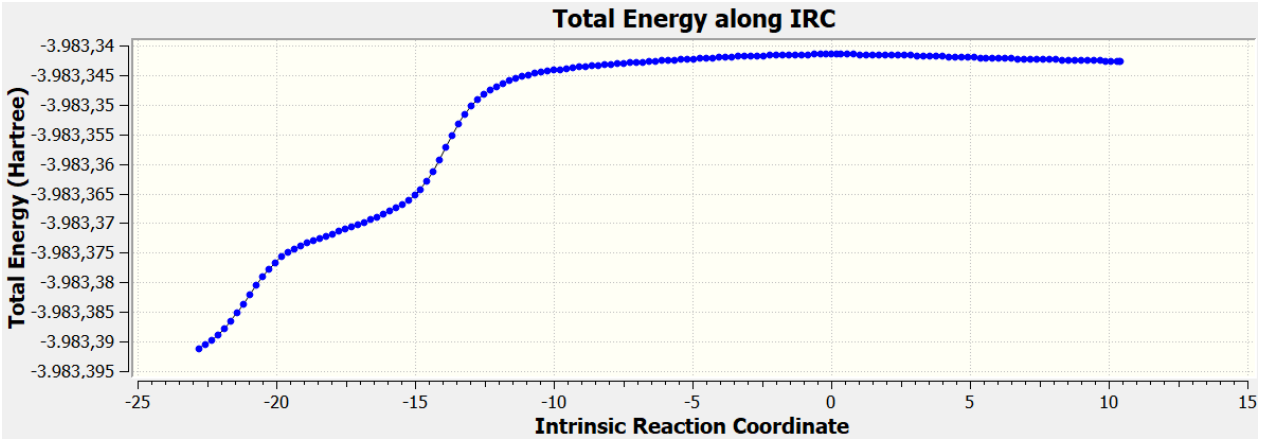

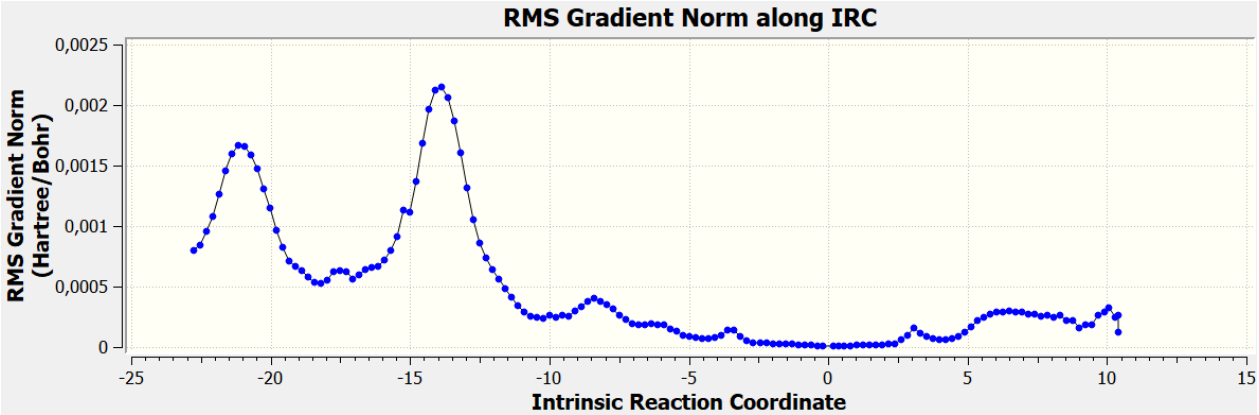

Fig. 21: IRC plot of the transition state **^{1}tsI** demonstrating an asynchronous concerted reaction pathway.

Table S14: Key geometric parameters for the optimized structures of the proposed reaction mechanism of the aziridination reaction (styrene with **N1^{+}**) obtained at TPSSh/def2-SVP and the empirical dispersion correction with Becke-Johnson damping level of theory level of theory.

	^{3}tsI	**^{3}tsII**	**^{3}IntI**	**^{3}IntII**	**^{1}tsI**	**^{1}intII**
bond lengths [Å]						
Cu – N(Pz. Pz')	2.112/2.173	2.081/2.185	2.060/2.222	2.079/2.170	2.054/2.273	2.073/2.151
Cu – N(Py)	2.061	1.933	2.033	1.922	1.988	2.179
Cu – $N_{nitrene}$	1.972	2.110	2.033	2.157	1.898	2.036
Cu – O	2.101	2.066	2.043	2.084	1.918	2.886
$N_{nitrene}$ – $C1_{styrene}$	2.418	1.475	1.478	1.483	3.326	1.481
$N_{nitrene}$ – $C2_{styrene}$	2.868	1.767	2.484	1.525	2.955	1.530
Valence angles [°]						
$N_{nitrene}$ – $C1_{styrene}$ – $C2_{styrene}$	94.4	73.8	112.9	62.1	62.4	62.4

Table S15: Comparison of single point (**SP**) energies of the optimized (**Geoopt**) structures **N1^{+}** + styrene and **^{3}intI** at different level of theory. The Gibbs free energy is stated relative to nitrene **N1^{+}** (triplet state) + styrene, which is set to 0.0 kcal/mol[1].

	ΔG N1^{+} + styrene / kcal · mol^{-1}	**ΔG ^{3}intI** / kcal · mol^{-1}
Geoopt1: TPSSh+D3(BJ)/def2-SVP		
SP1: TPSSh/def2-SVP	0.0	–21.3
SP2: TPSSh/def2-TZVP	0.0	–14.7
SP3: TPSSh/def2-QZVPP	0.0	–14.8
SP4: DLPNO-CCSD(T)/def2-SVP	0.0	–23.5
SP5: DLPNO-CCSD(T)/def2-TZVP	0.0	–23.4
Geoopt2: TPSSh+D3(BJ)/def2-TZVP		
SP6: TPSSh/def2-TZVP	0.0	–15.5
SP7: DLPNO-CCSD(T)/def2-SVP	0.0	–24.3

Discussion of

Table S15:

The ΔΔG values of the structures optimized at a different level of theory lead to only small differences in the calculated energies (**SP2** vs. **SP6**: ΔΔG = 0.8 kcal · mol^{-1}; **SP4** vs **SP7**: ΔΔG = 0.9 kcal · mol^{-1}). Hence, it can be assumed that the structures optimized with **Geoopt1** and **Geoopt2** differ only slightly in their geometries. However, large differences in the calculated energies are obtained for the same structure in dependence on the chosen level of theory. The energies obtained with DLPNO-CCSD(T) calculations (**SP4**), which are known to produce accurate energies, differ enormously compared to the calculated energy at the TPSSh/def2-QZVPP (**SP3**) and TPSSh/def2-

TZVP (**SP2**) level of theory ($\Delta\Delta G$ = 8.7 kcal · mol^{-1}). To rule out inaccuracies in the DLPNO-CCSD(T) calculations due to the chosen basis set def2-SVP, the calculations were repeated with the larger basis set def2-TZVP, with no significant deviation. According to this, it can be assumed that for our complexes the DLPNO-CCSD(T) calculations produce very accurate energies even with the small basis set def2-SVP in contrast to the DFT calculations with the large basis set def2-QZVPP.

Deviations between the calculated structures at a different level of theory were analyzed with the program aRMSD [s2] using the default settings.

The structure of **N1**$^+$, calculated with TPSSh+D3(BJ)/def2-SVP, is in excellent agreement with that calculated with def2-TZVP basis set, with a total RMSD of 0.0666 Å. Only small deviations are due to twists of the two benzene groups (Fig. S22: Superposition with Root-Mean-Square-Deviation (RMSD) for the calculated structures of **N1**$^+$ at TPSSh+D3(BJ)/def2-SVP and def2-TZVP level of theory. The sphere dimensions reflect the relative RMSD distribution and the color code the absolute deviation (small for green color and large for red color).). The bond lengths are in excellent agreement, as evidenced with the RMSE of 0.012 Å (Fig. S23). A slight deviation is visible for the copper nitrene bond, which is elongated by 0.03 Å for the structure calculated with def2-SVP basis set.

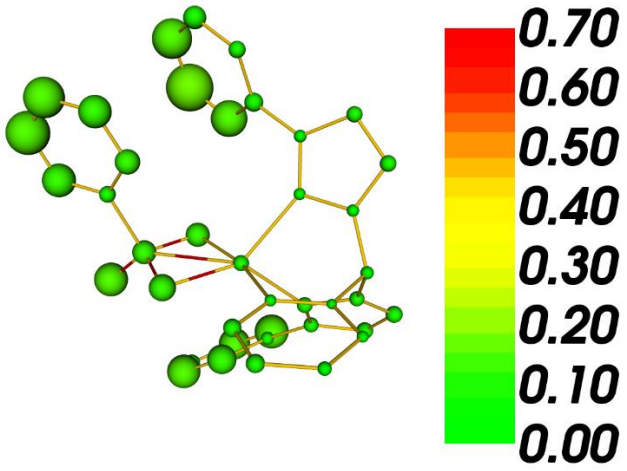

Fig. S22: Superposition with Root-Mean-Square-Deviation (RMSD) for the calculated structures of **N1**$^+$ at TPSSh+D3(BJ)/def2-SVP and def2-TZVP level of theory. The sphere dimensions reflect the relative RMSD distribution and the color code the absolute deviation (small for green color and large for red color).

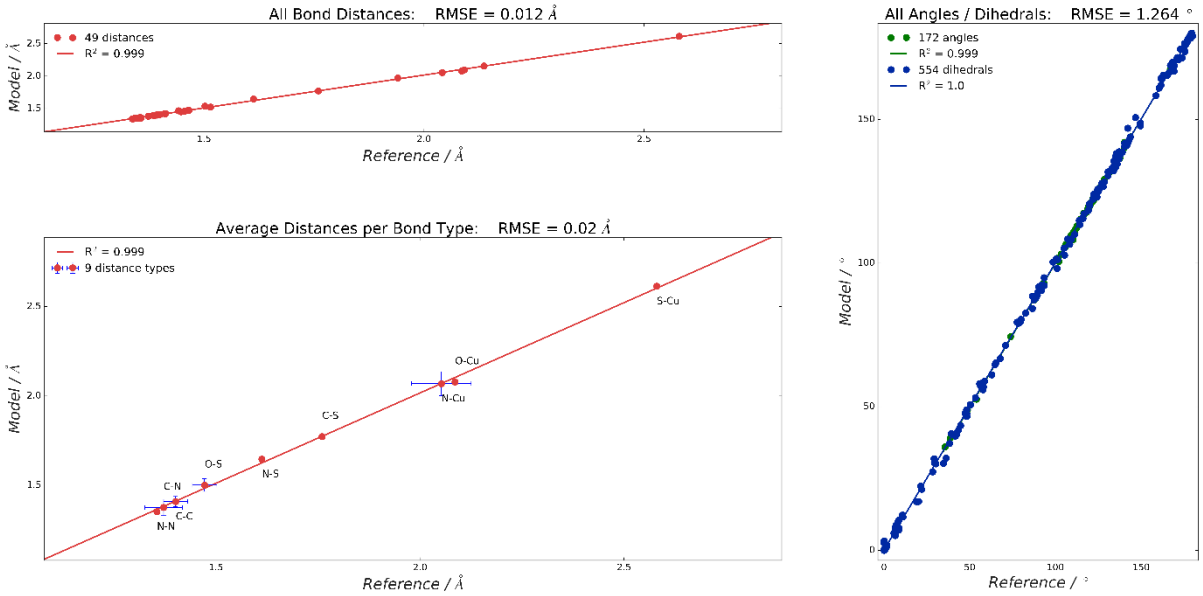

Fig. S23. Detailed analysis of the Root-Mean-Square-Error (RMSE) for bonds and angles for the calculated structures **N1**$^+$ at TPSSh+D3(BJ)/def2-SVP (model) and def2-TZVP level of theory (reference).

[s2] A. Wagner, H.-J. Himmel, *J. Chem. Inf. Model* **2017**, *57*, 428-438.

The structure of **^{3}intI**, calculated with TPSSh+D3(BJ)/def2-SVP, is in very good agreement with that calculated with def2-TZVP basis set, with a total RMSD of 0.205 Å. The main deviation is due to a twist of the benzene group of the styrene (Fig. S24). The bond lengths are in excellent agreement, as evinced with the RMSE of 0.013 Å (Fig. S25). A slight deviation is visible for the copper nitrene bond, which is elongated by 0.02 Å for the structure calculated with def2-SVP basis set.

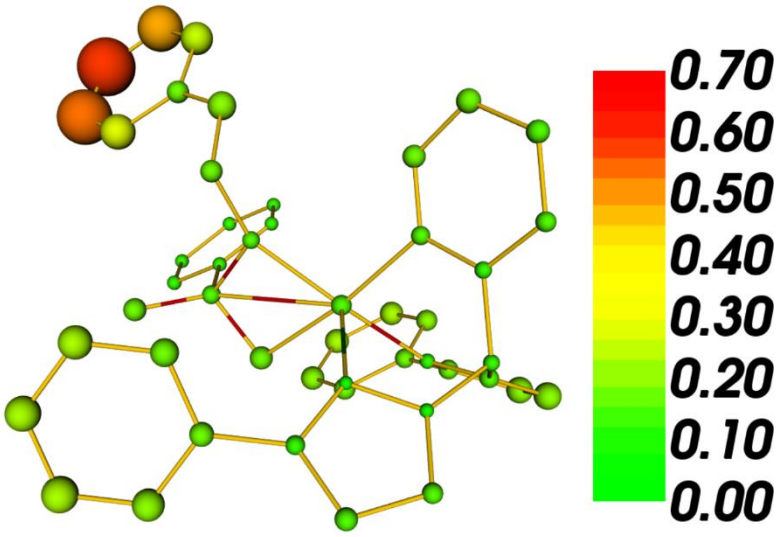

Fig. S24. Superposition with Root-Mean-Square-Deviation (RMSD) for the calculated structures of **^{3}intI** at TPSSh+D3(BJ)/def2-SVP and def2-TZVP level of theory. The sphere dimensions reflect the relative RMSD distribution and the color code the absolute deviation (small for green color and large for red color).

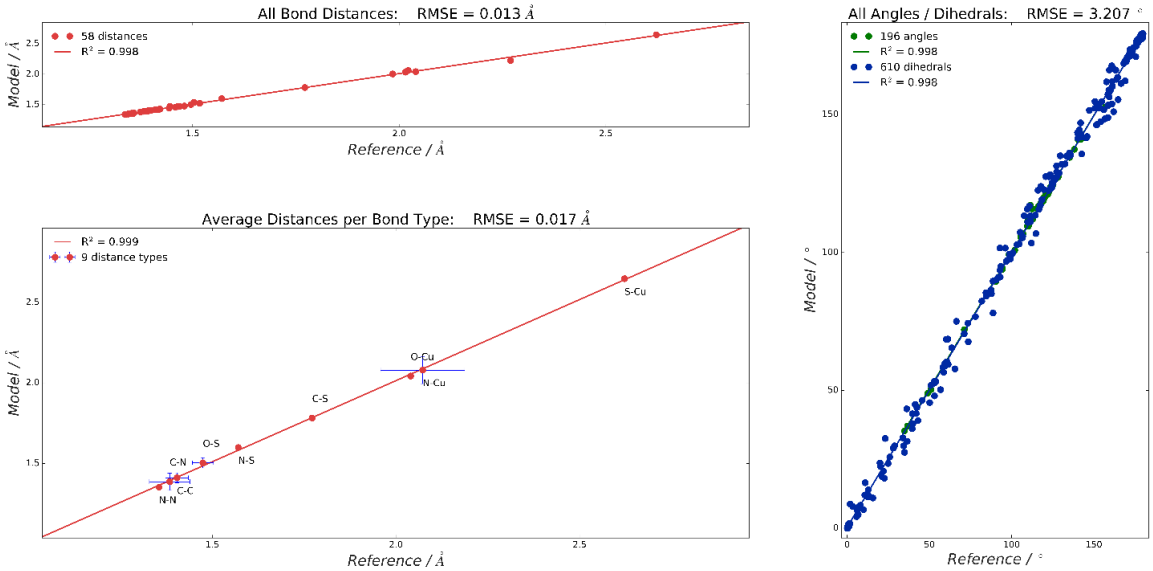

Fig. S25. Detailed analysis of the Root-Mean-Square-Error (RMSE) for bond lenghts and angles for the calculated structures **^{3}intI** at TPSSh+D3(BJ)/def2-SVP (model) and def2-TZVP level of theory (reference).

6. NMR data

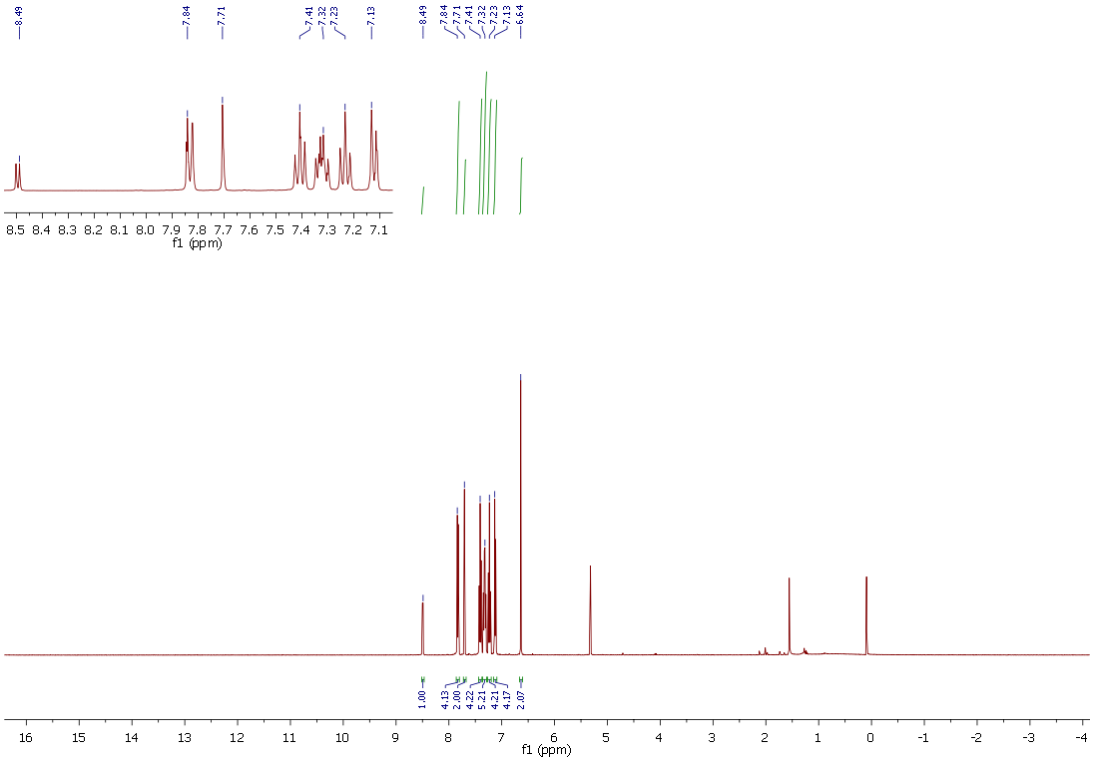

Fig. S26: ^{1}H-NMR spectrum of **L2** in DCM-d_2.

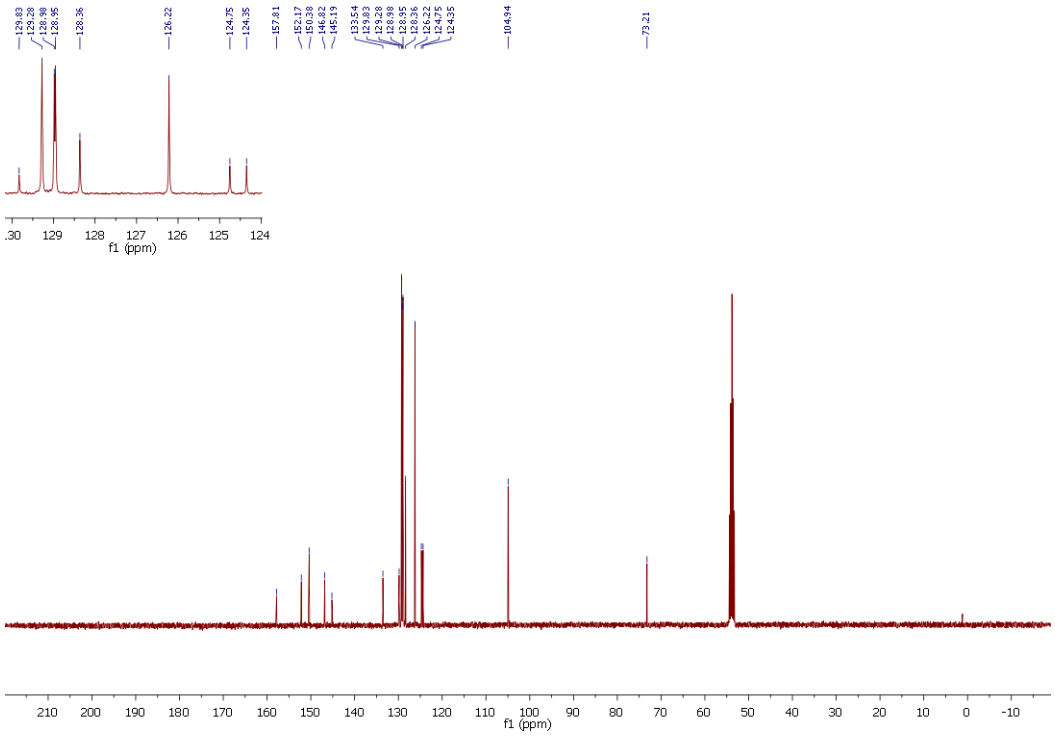

Fig. S27: ^{13}C-{^{1}H}-NMR spectrum of **L2** in DCM-d_2.

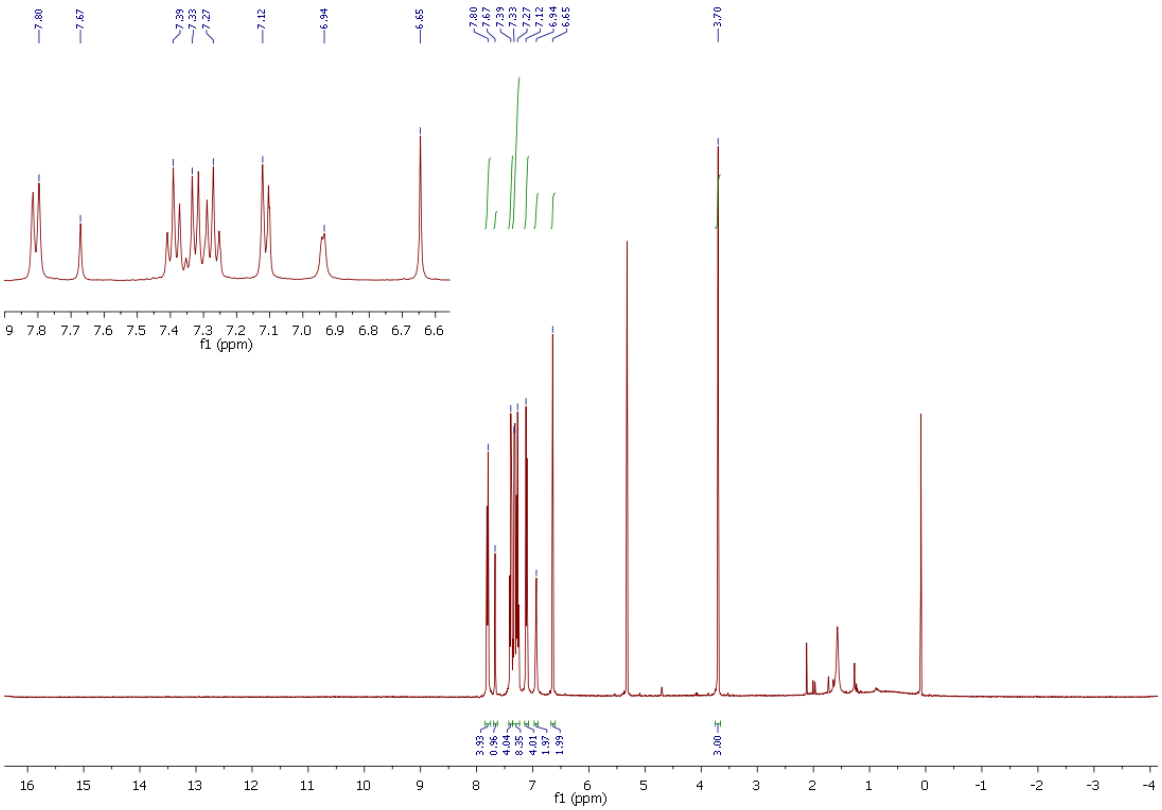

Fig. S28: ^{1}H-NMR spectrum of **L3** in DCM-d_2.

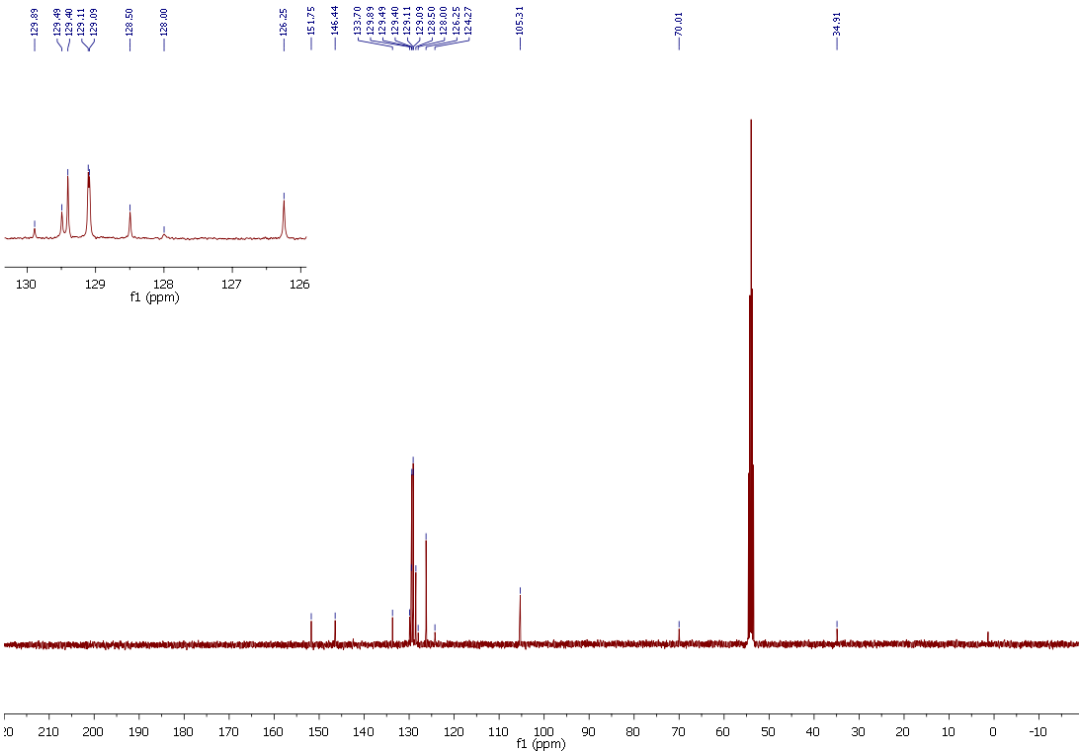

Fig. S29: ^{13}C-{^{1}H}-NMR spectrum of **L3** in DCM-d_2.

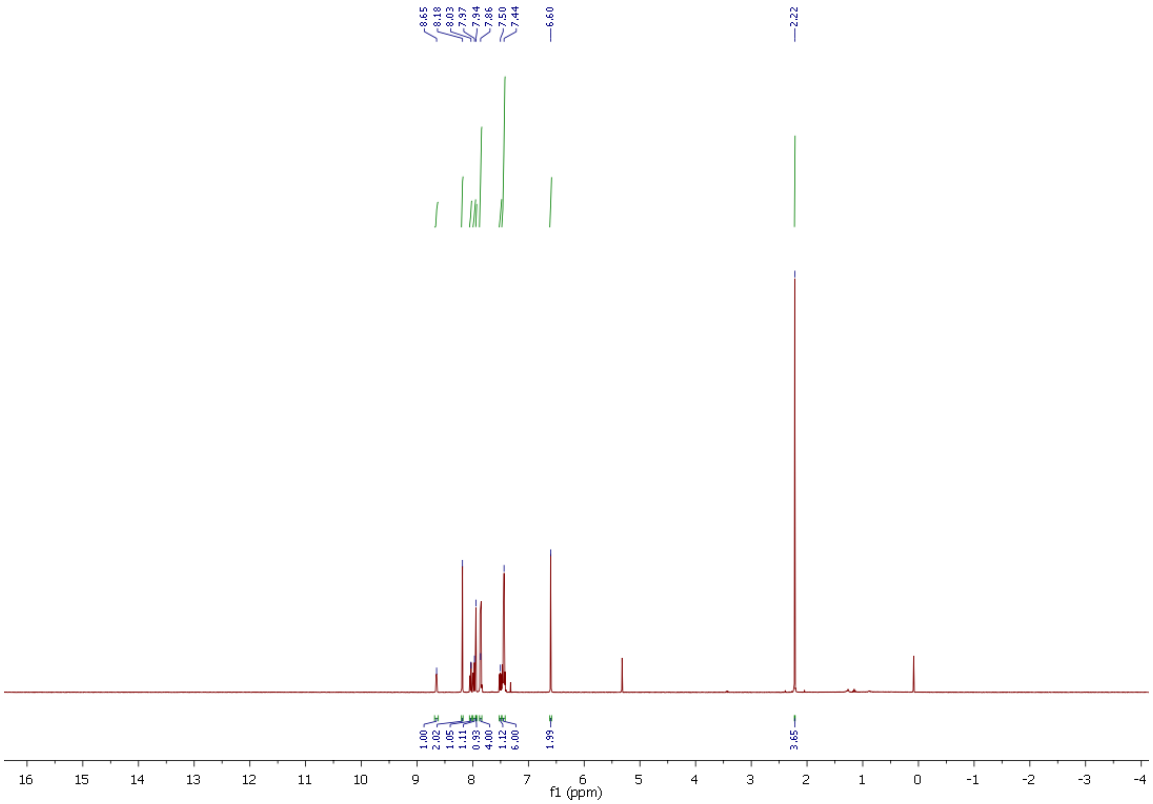

Fig. S30: ^{1}H-NMR spectrum of **C1** in DCM-d_2.

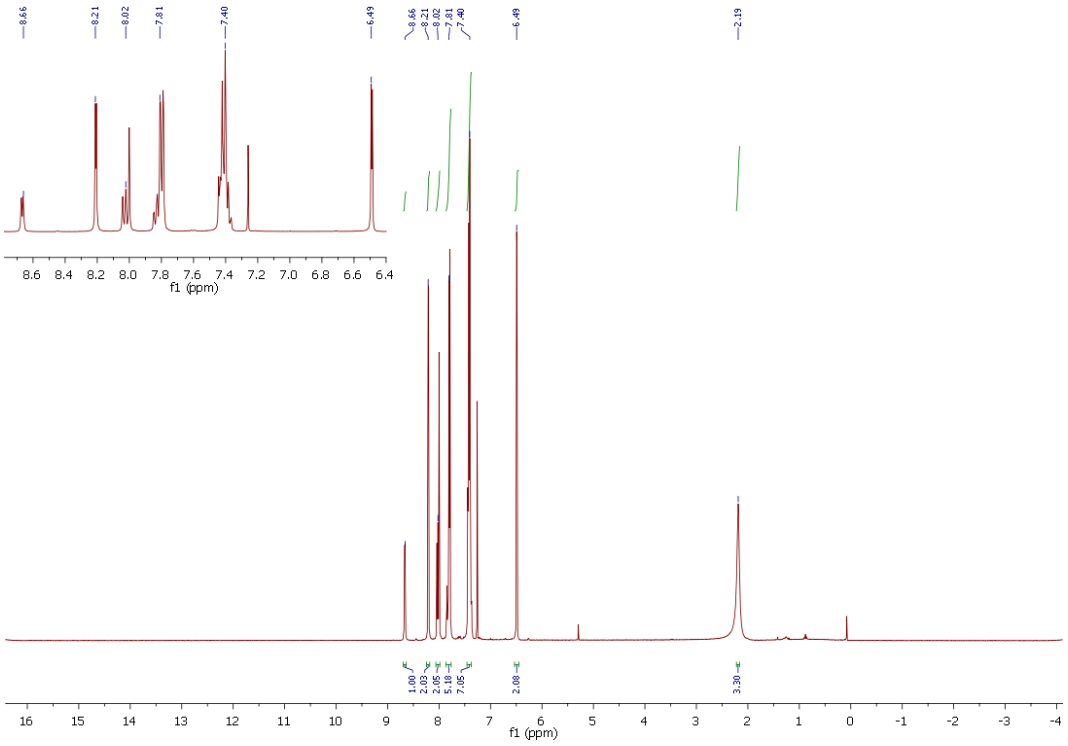

Fig. S31: ^{1}H-NMR spectrum of **C1** in $CDCl_3$.

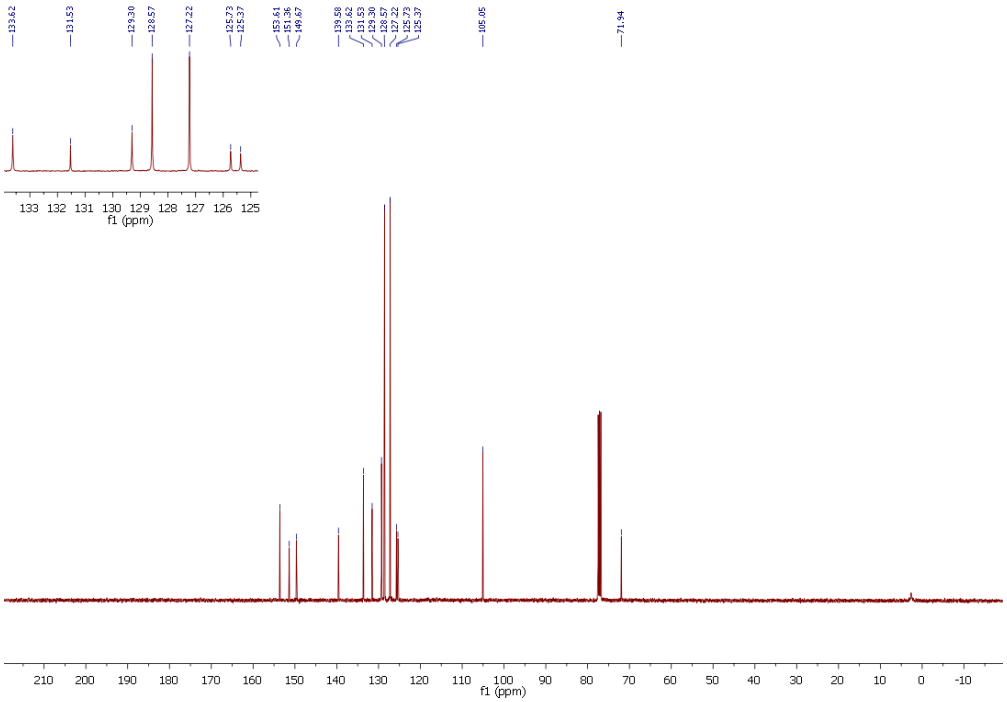

Fig. S32: ^{13}C-{^{1}H}-NMR spectrum of **C1** in $CDCl_3$.

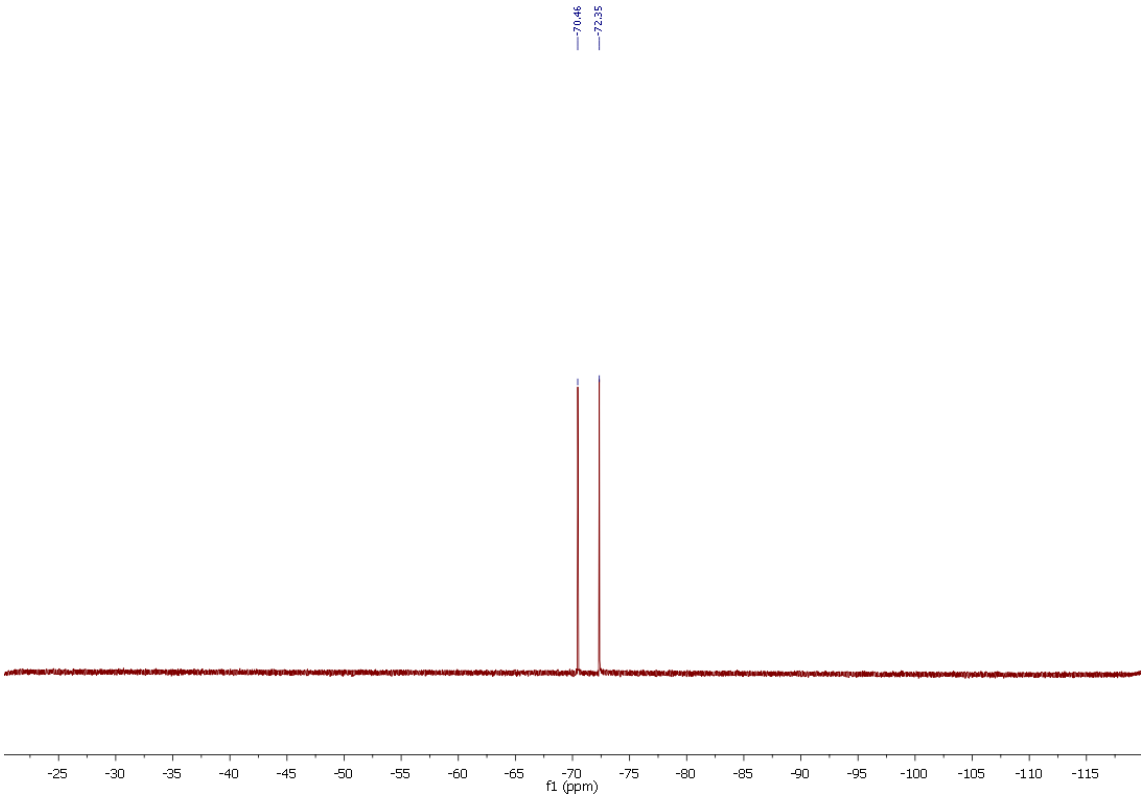

Fig. S33: ^{19}F-{^{1}H}-NMR spectrum of **C1** in $CDCl_3$.

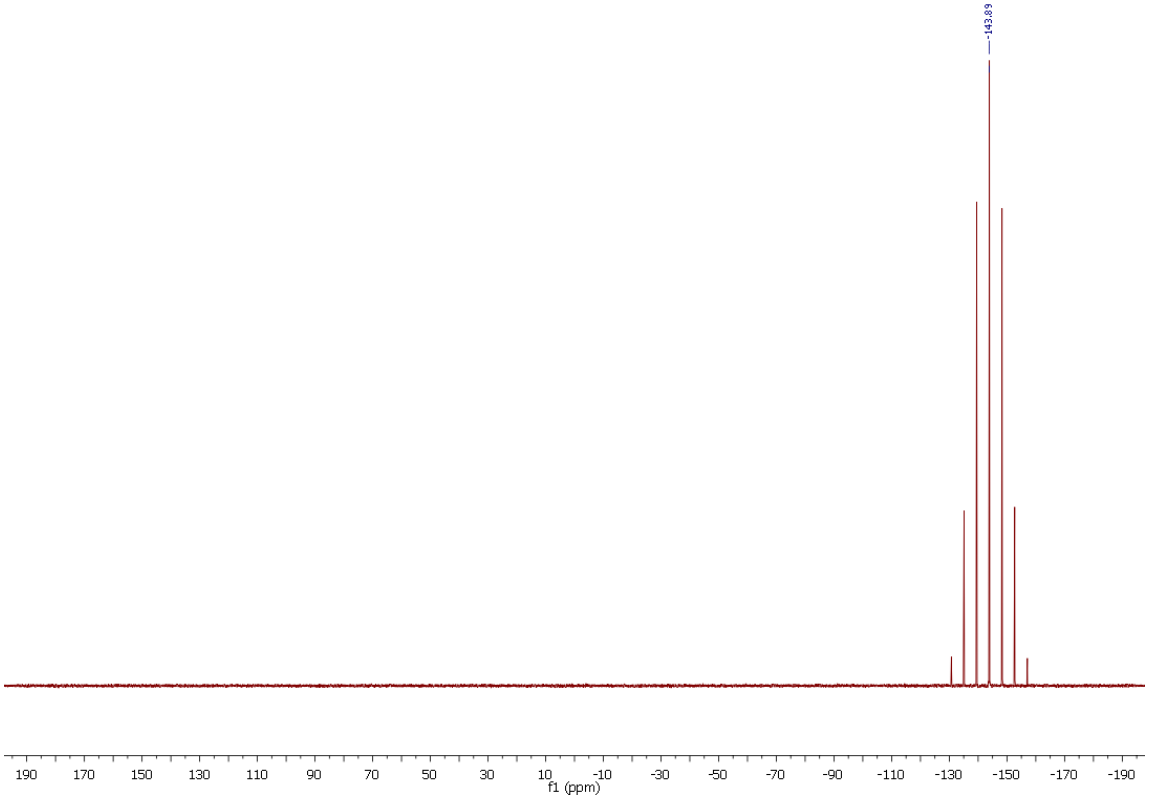

Fig. S34: ^{31}P-{^{1}H}-NMR spectrum of **C1** in $CDCl_3$.

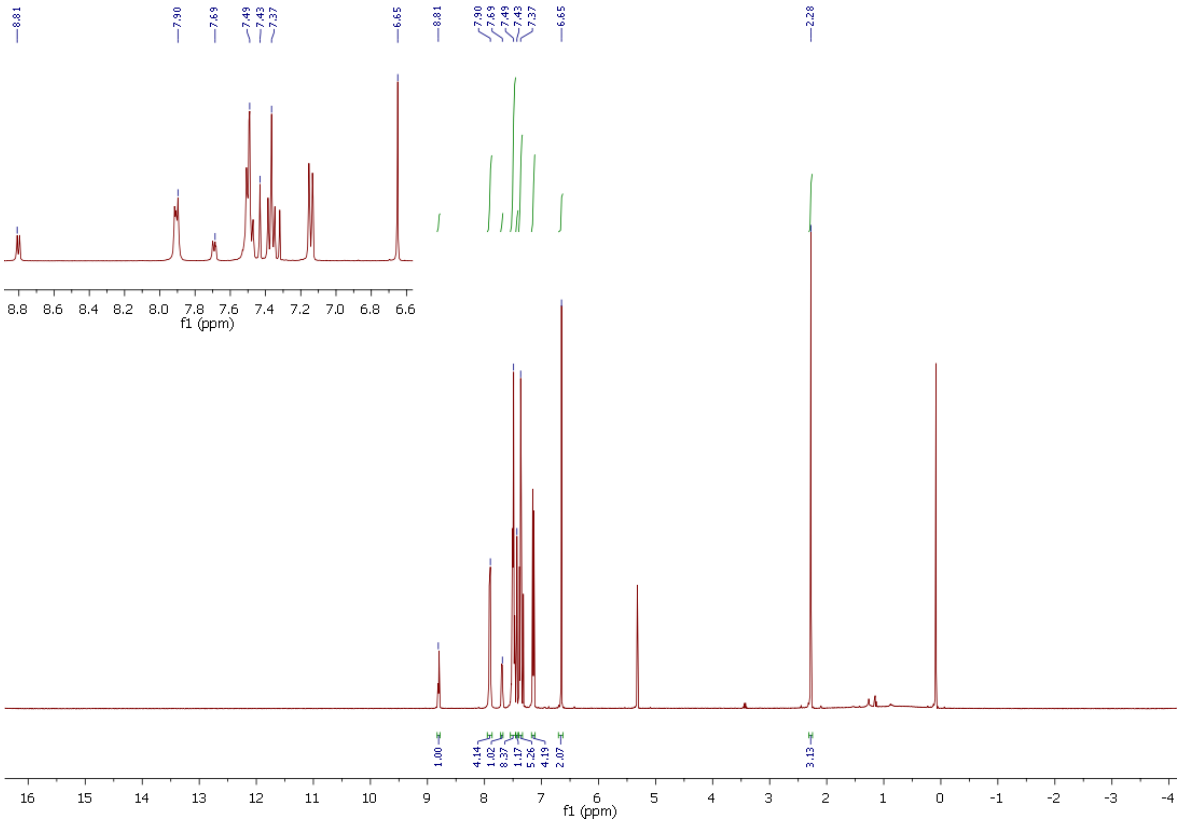

Fig. S35: ^{1}H-NMR spectrum of **C2** in DCM-d_2.

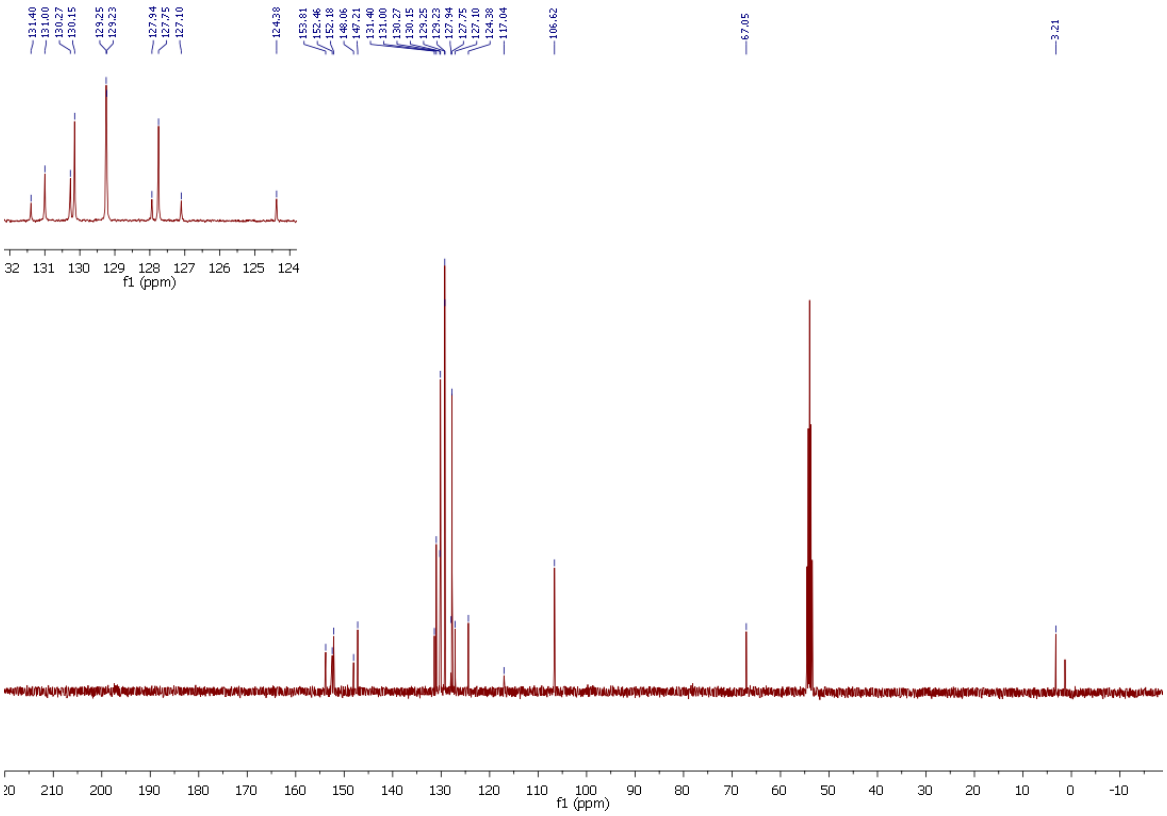

Fig. S36: ^{13}C-{^{1}H}-NMR spectrum of **C2** in DCM-d_2.

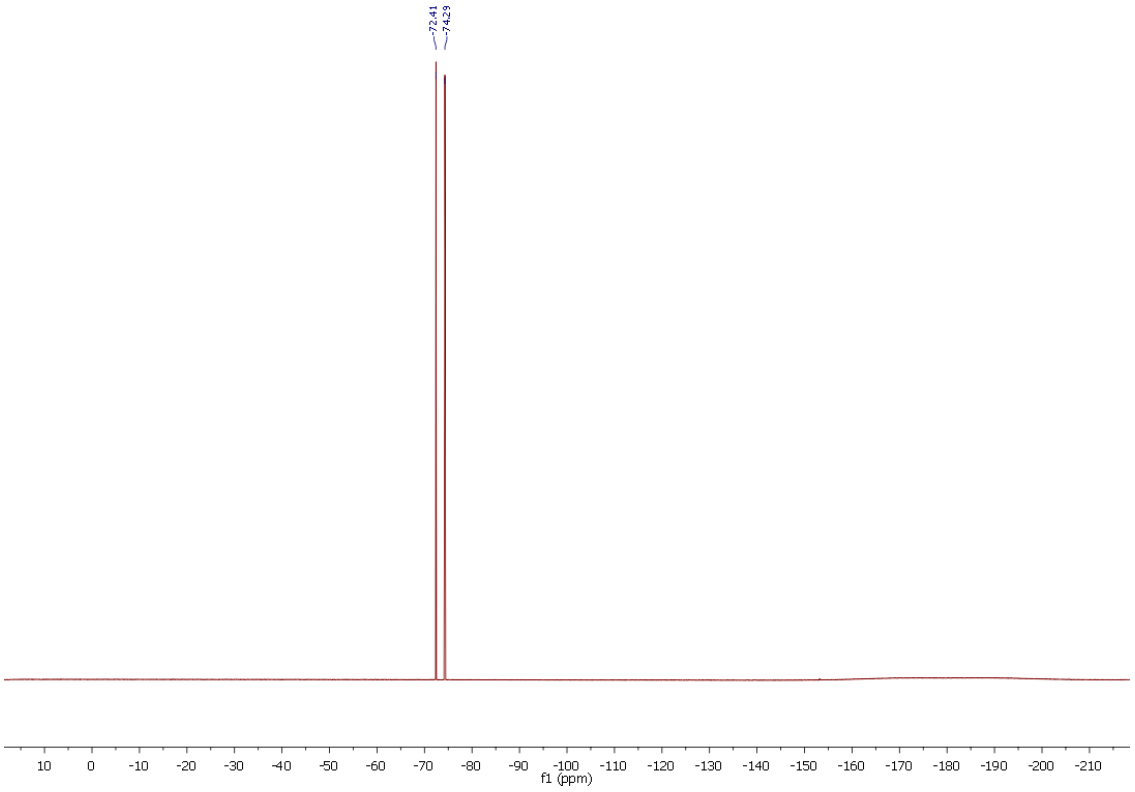

Fig. S37: ^{19}F-{^{1}H}-NMR spectrum of **C2** in DCM-d_2.

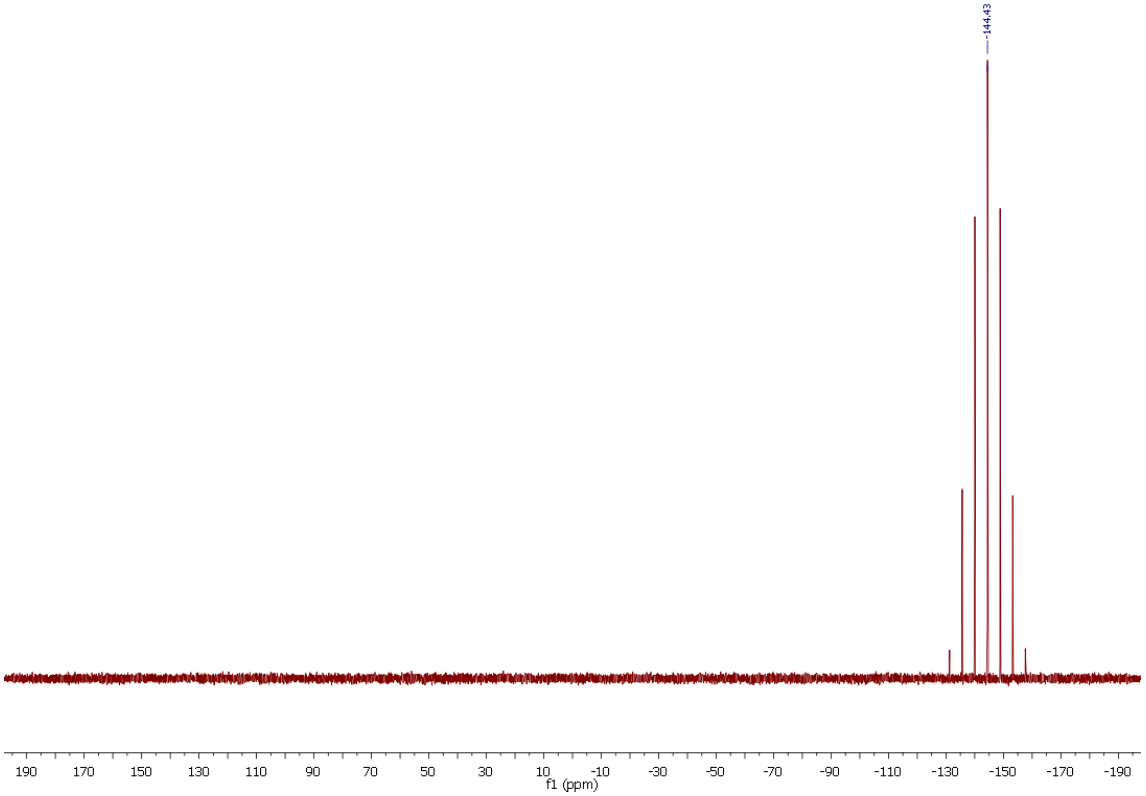

Fig. S38: ^{31}P-{^{1}H}-NMR spectrum of **C2** in DCM-d_2.

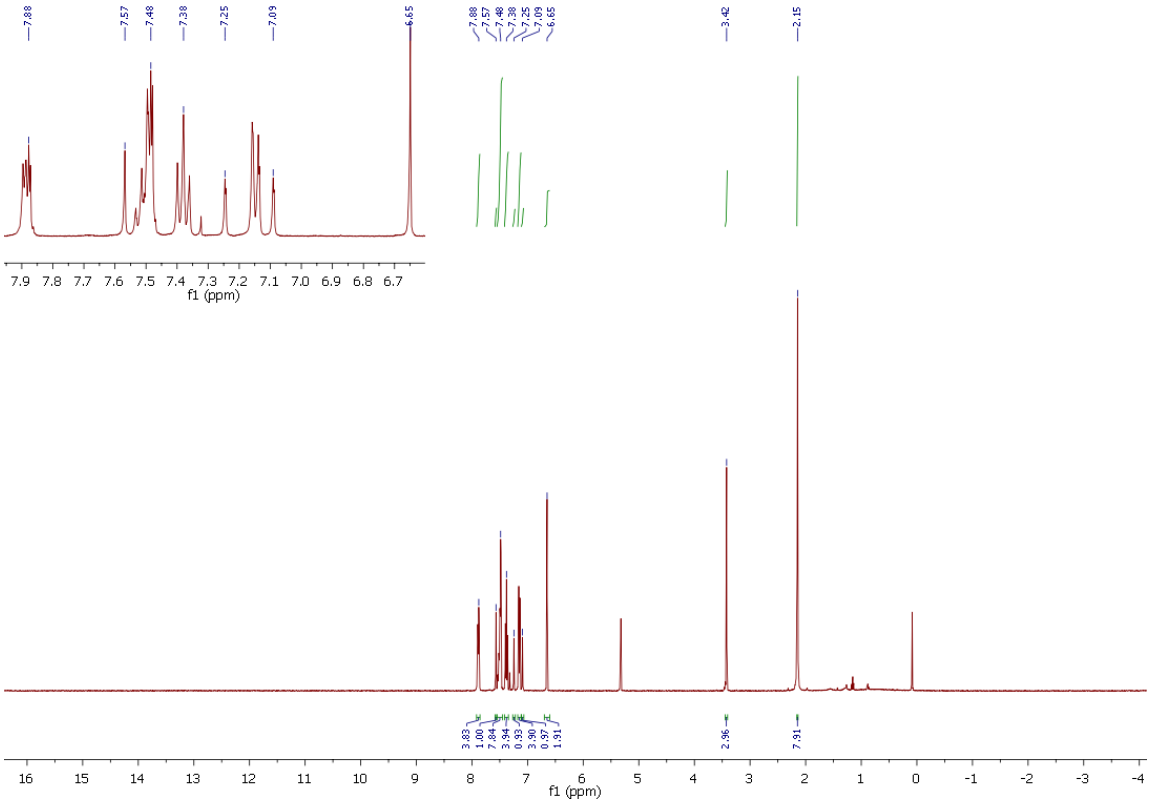

Fig. S39: ^{1}H-NMR spectrum of **C3** in DCM-d_2.

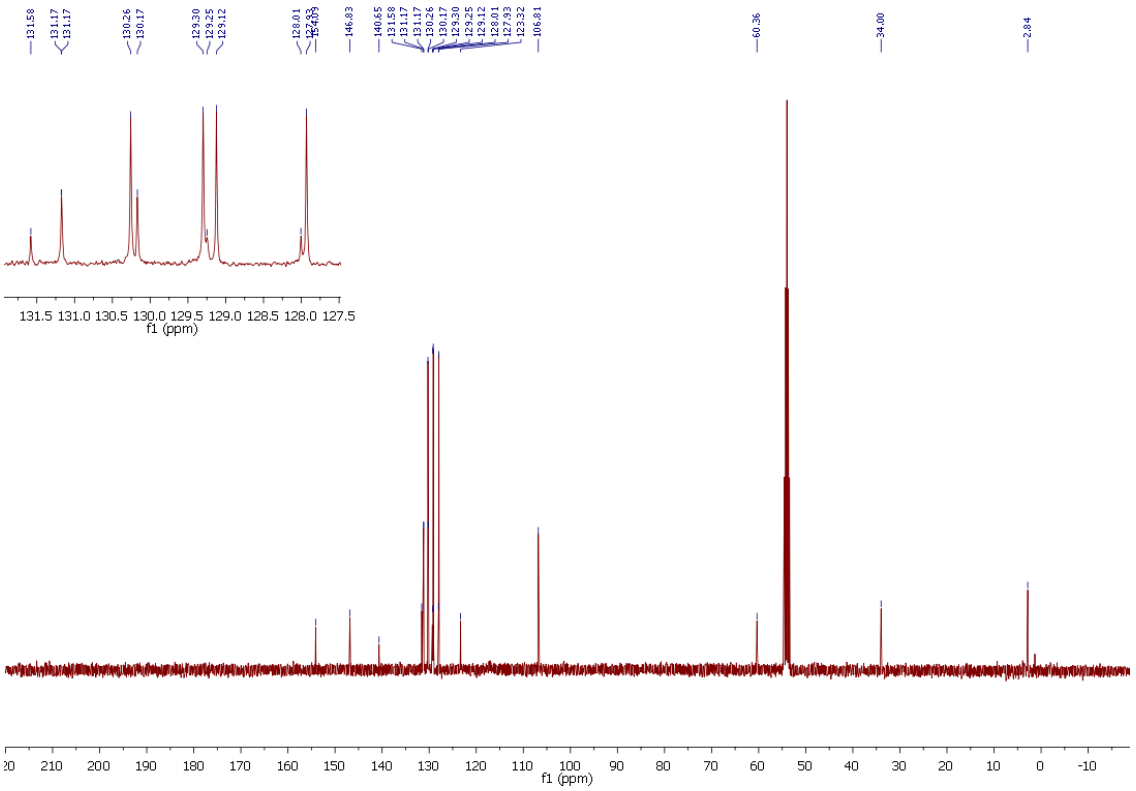

Fig. S40: ^{13}C-{^{1}H}-NMR spectrum of **C3** in DCM-d_2.

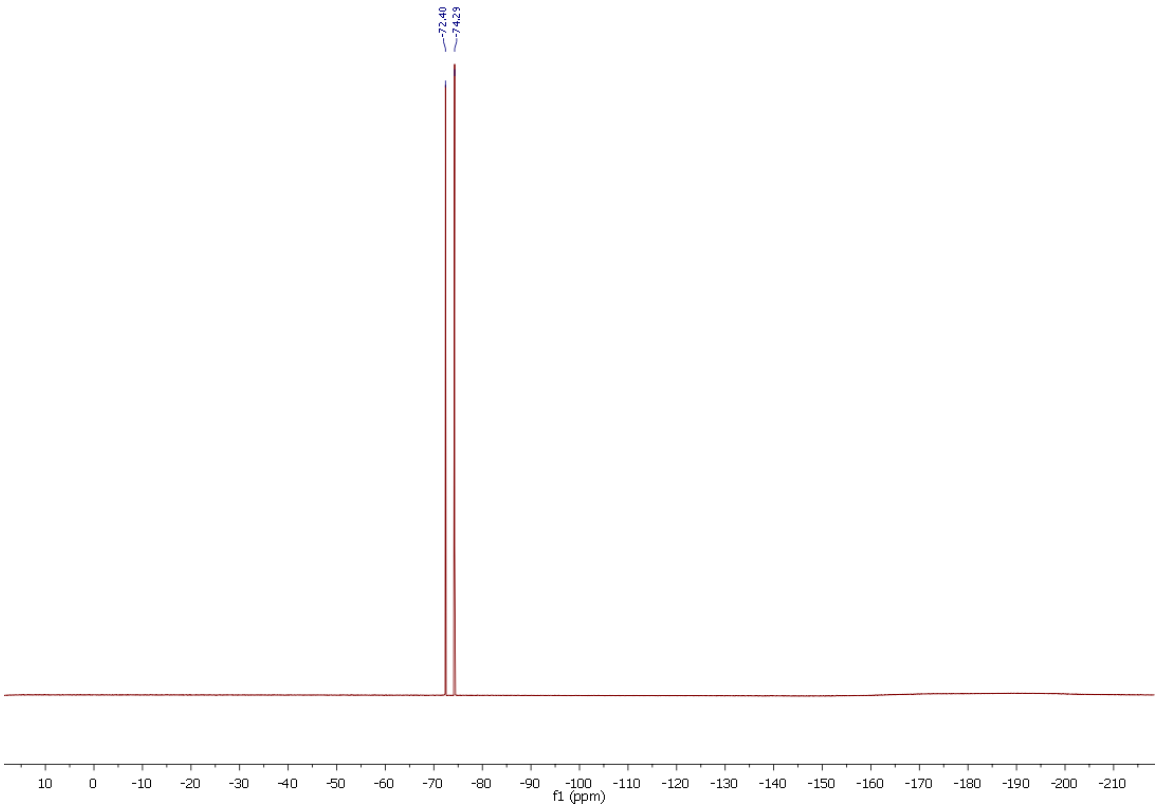

Fig.S41: ^{19}F-{^{1}H}-NMR spectrum of **C3** in DCM-d_2.

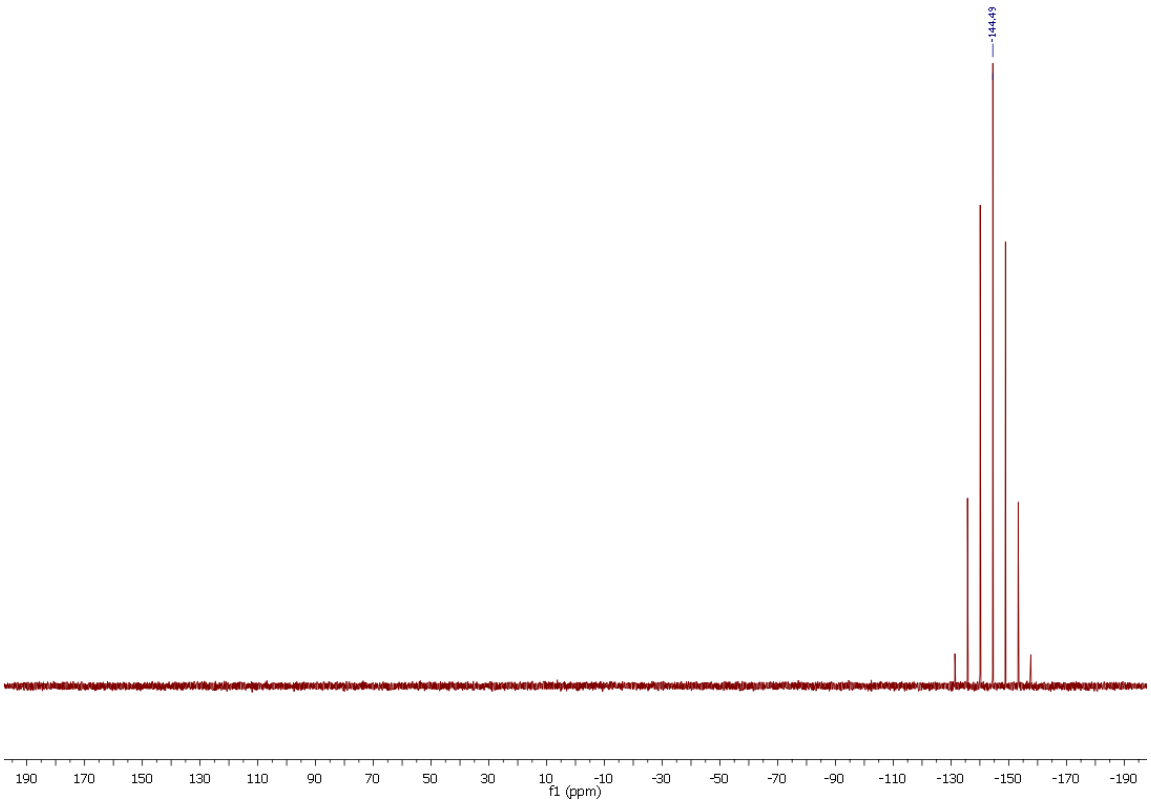

Fig. S42: ^{31}P-{^{1}H}-NMR spectrum of **C3** in DCM-d_2.

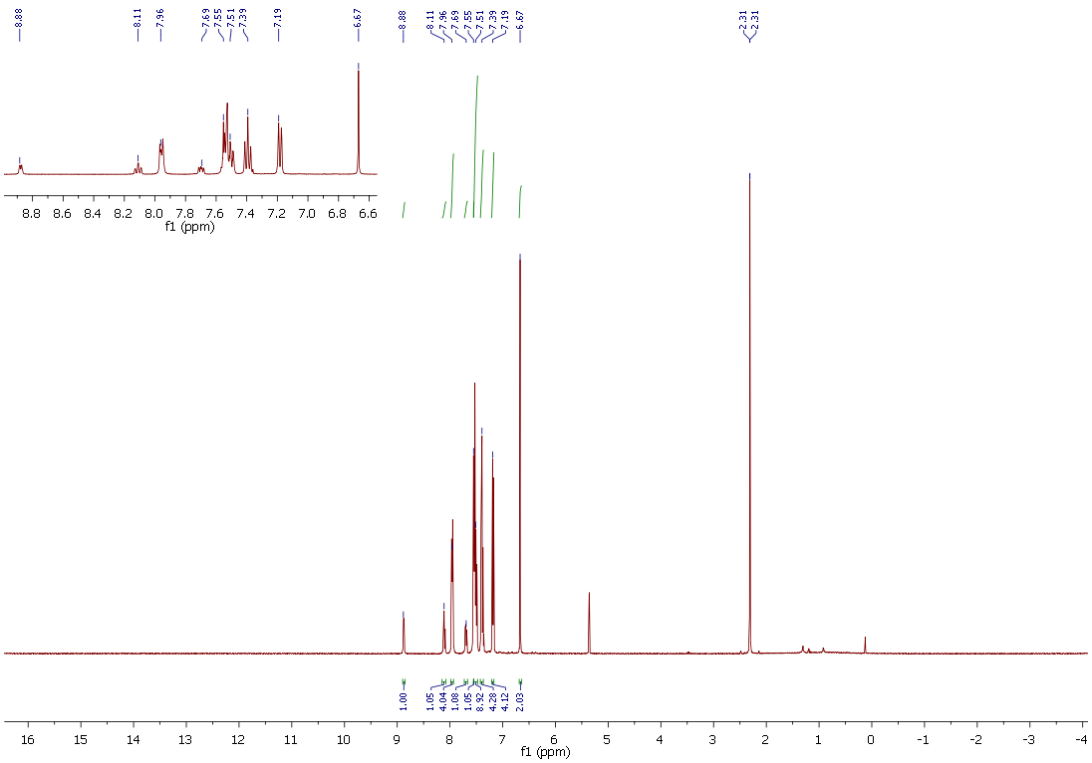

Fig. S43: ^{1}H-NMR spectrum of **C4** in DCM-d_2.

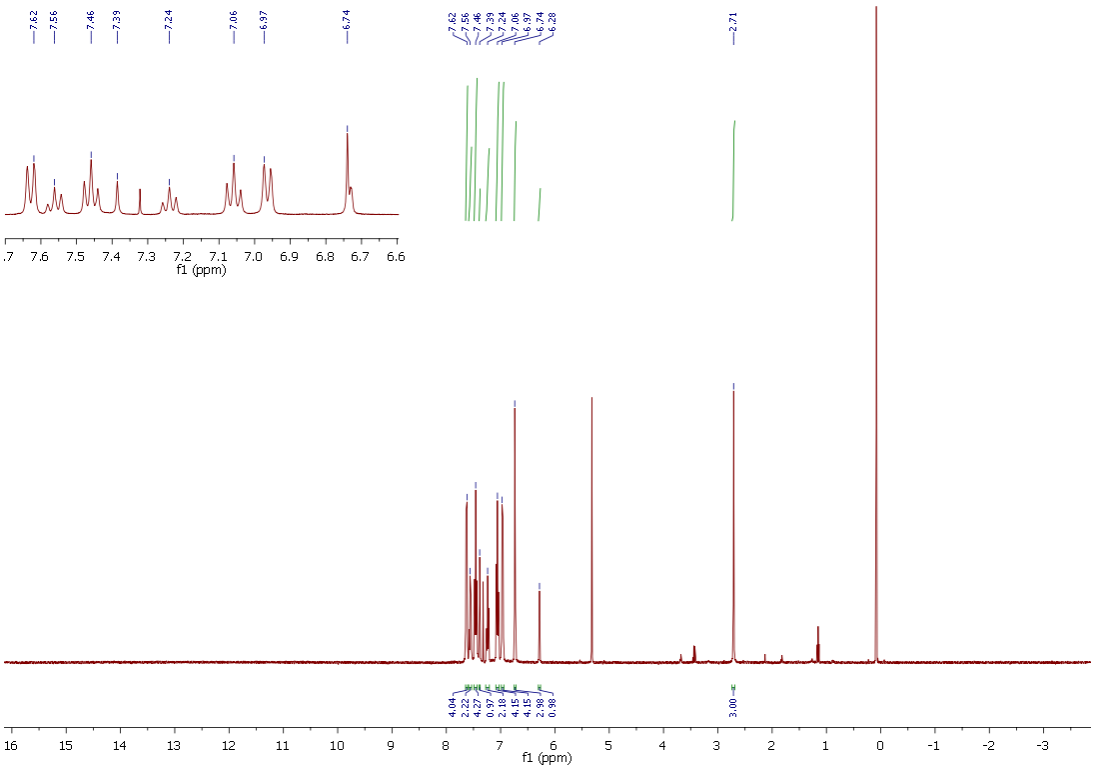

Fig. S44: ^{1}H-NMR spectrum of **C5** in DCM-d_2.

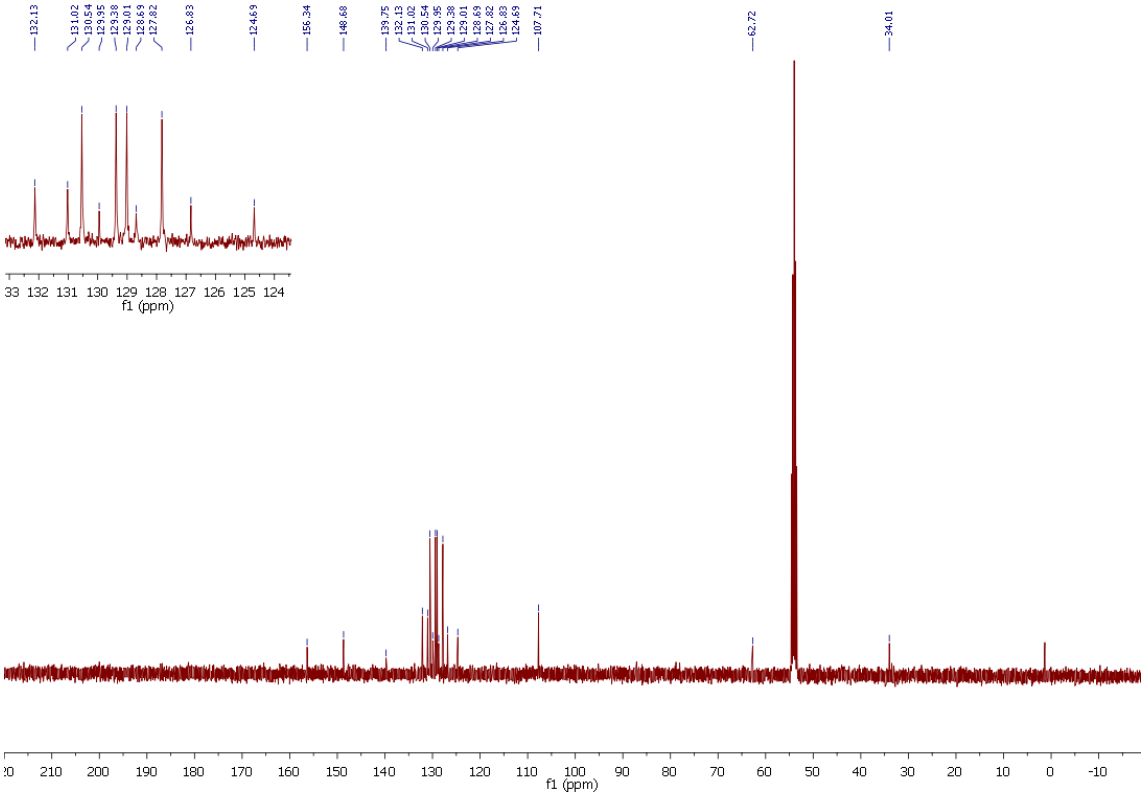

Fig. S45: ^{13}C-{^{1}H}-NMR spectrum of **C5** in DCM-d_2.

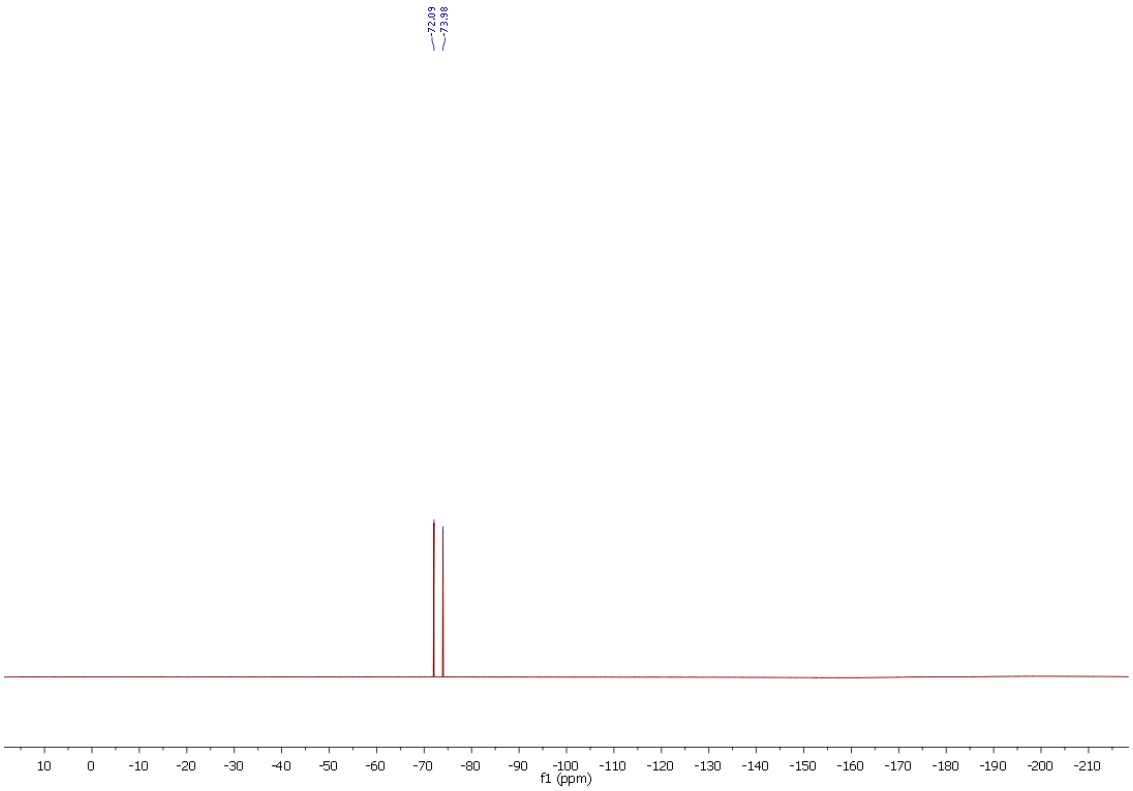

Fig. S46: ^{19}F-{^{1}H}-NMR spectrum of **C5** in DCM-d_2.

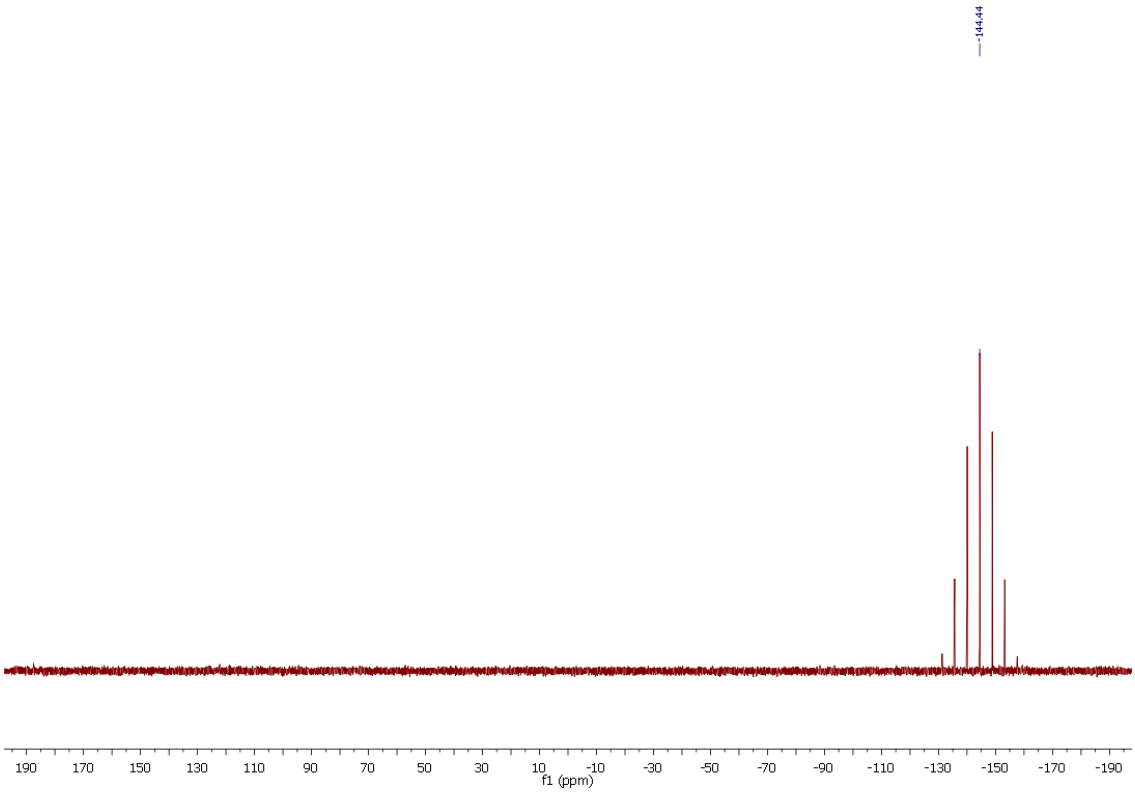

Fig. S47: ^{31}P-{^{1}H}-NMR spectrum of **C5** in DCM-d_2.

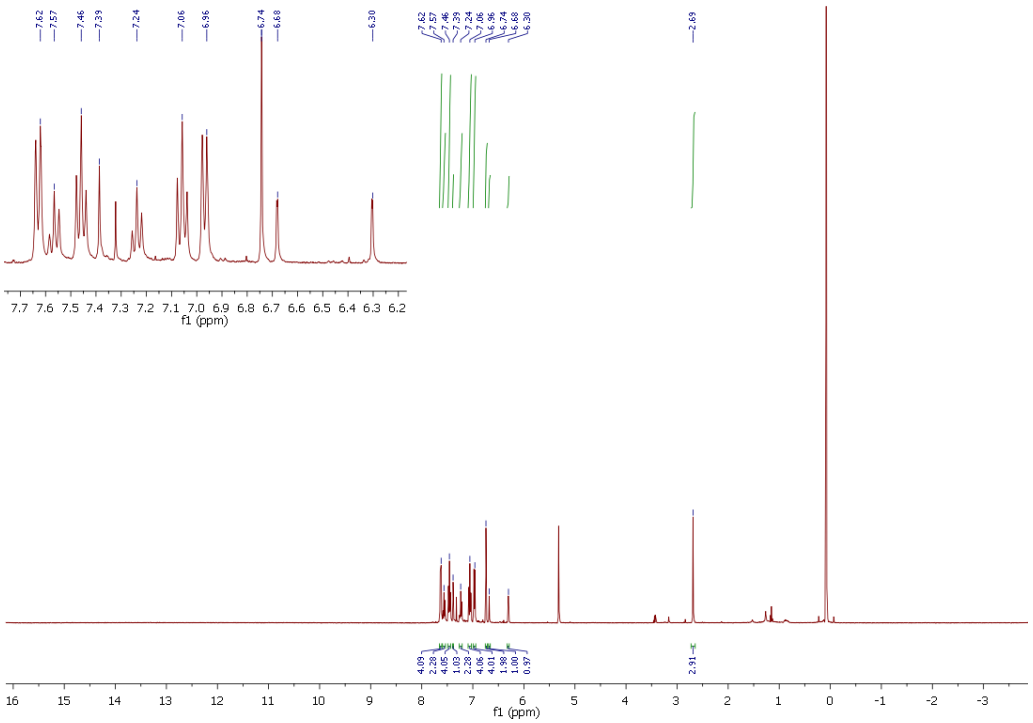

Fig. S48: ^{1}H-NMR spectrum of **C6** in DCM-d_2.

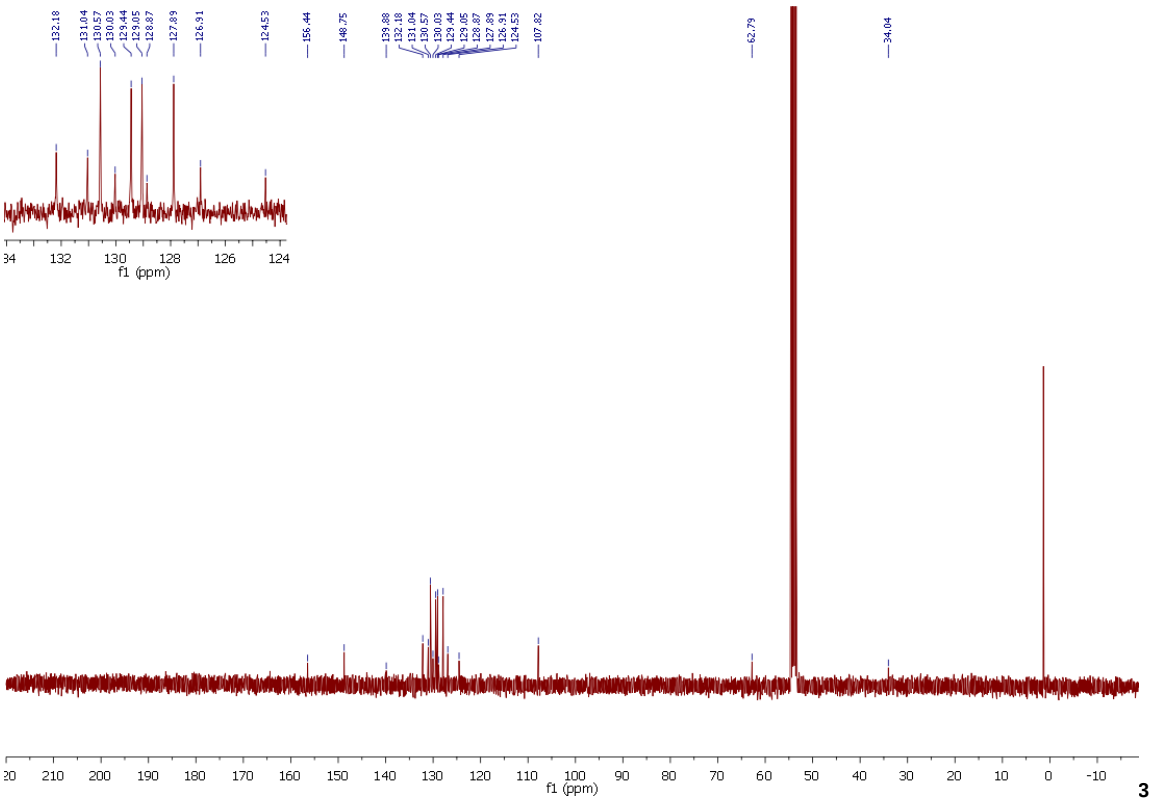

3

Fig. S49: ^{13}C-{^{1}H}-NMR spectrum of **C6** in DCM-d_2.

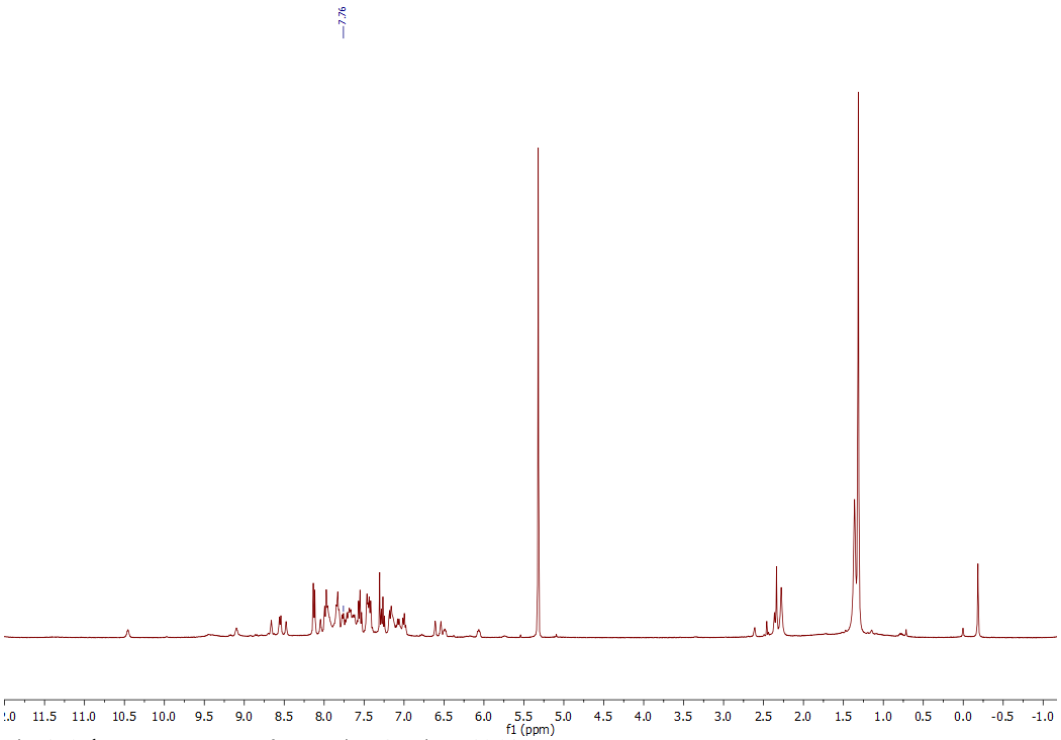

Fig. S50: ^{1}H-NMR spectrum of **N1PF$_6$** in DCM-d$_2$ at -80 °C.

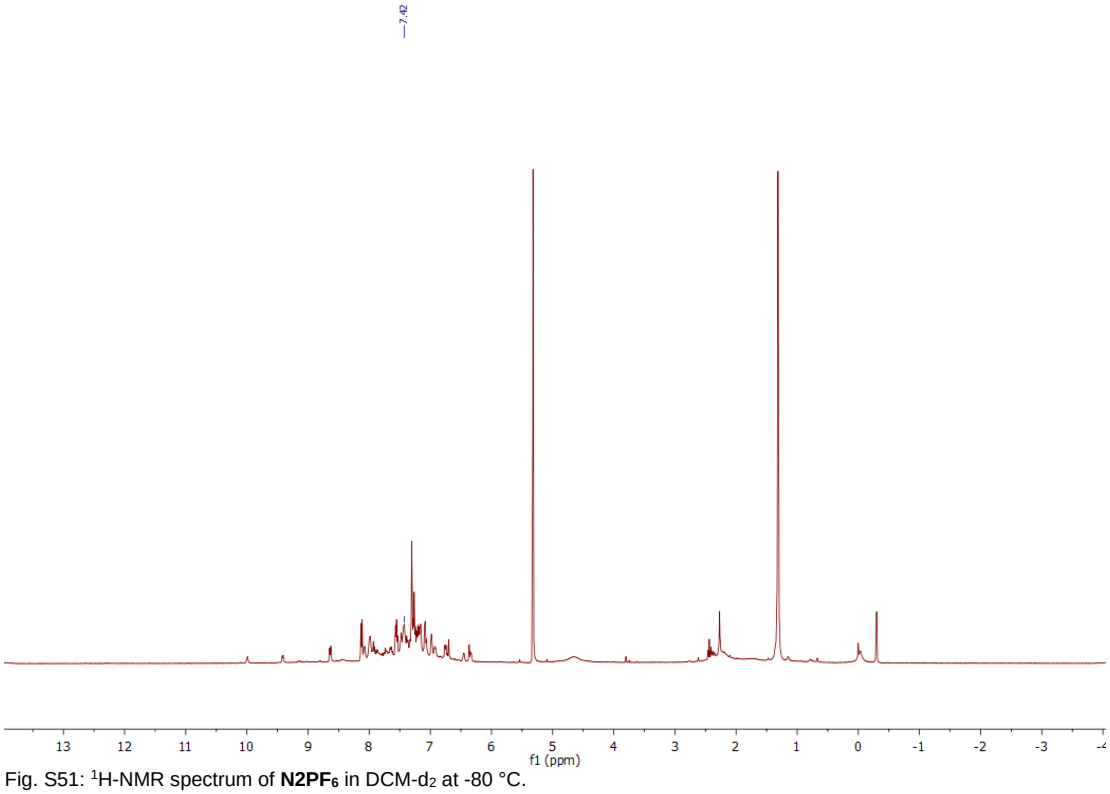

Fig. S51: ^{1}H-NMR spectrum of **N2PF$_6$** in DCM-d$_2$ at -80 °C.

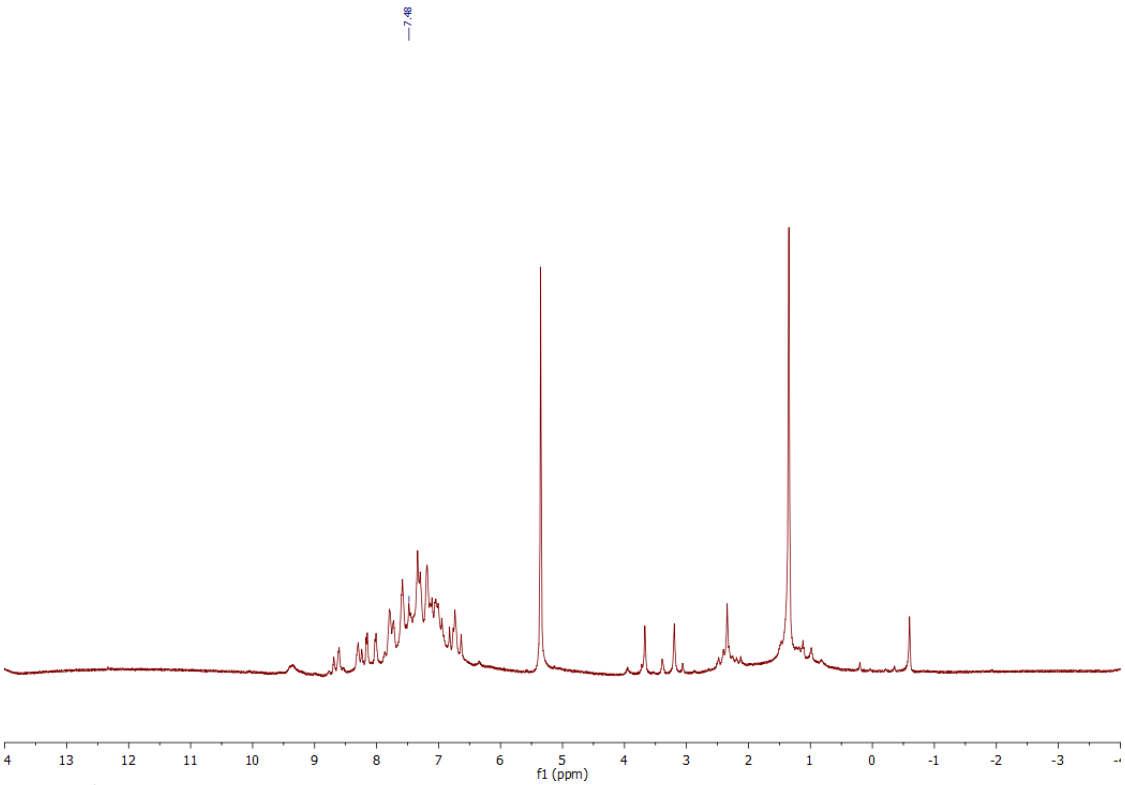

Fig. S52: ^{1}H-NMR spectrum of **N3PF$_6$** in DCM-d$_2$ at -80 °C.

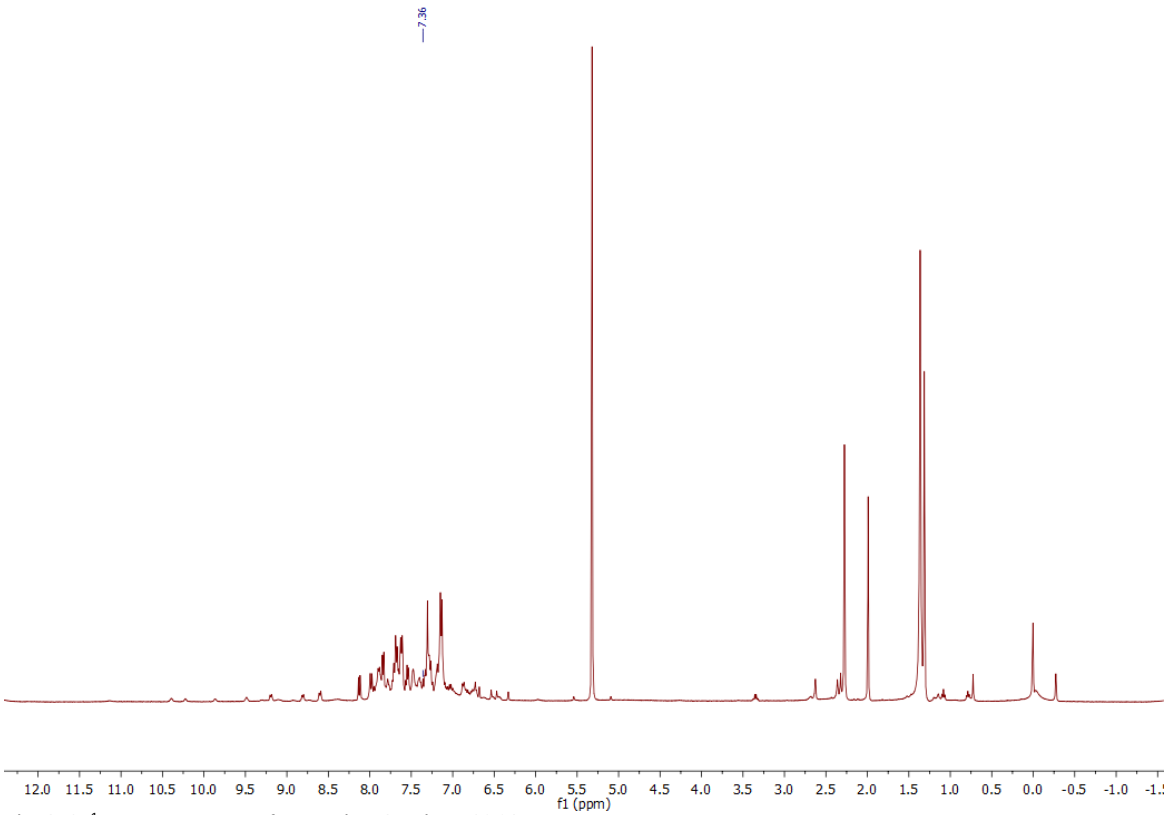

Fig. S53: ^{1}H-NMR spectrum of **N4PF$_6$** in DCM-d$_2$ at -80 °C.

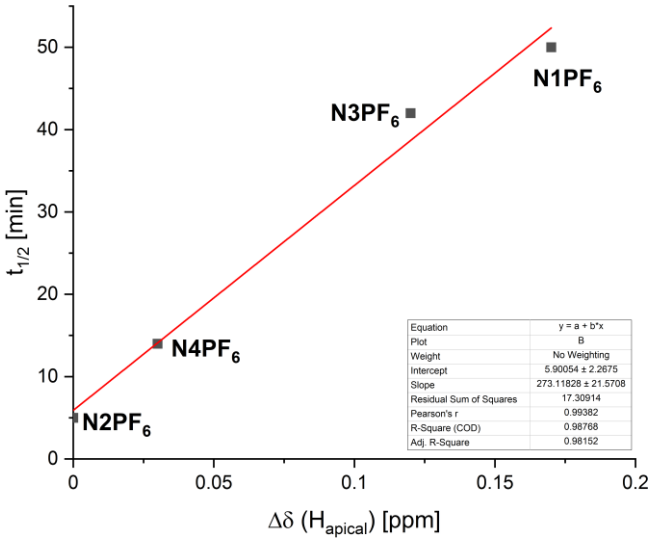

Fig. S54: Plot of nitrene half-life time and the different in the shift of the apical hydrogen atom.